ADVANCED HEALTHCARE MATERIALS
www.advhealthmat.de

β-1,3 Glucan Microparticles & Nanoparticles: Fabrication Methods & Applications in Immunomodulation & Targeted Drug Delivery

*Nate Dowdall and Todd Hoare**

Innate immune cells such as macrophages and dendritic cells play major roles in the progression of many cancerous, fibrotic, and autoimmune diseases, often due to environmental cues that skew these cells toward a phenotype that progresses or exacerbates the disease state. As such, a growing focus in treating such diseases is placed on exploiting the high plasticity of these cells to modify or reverse their pro-disease phenotypes using immunomodulatory materials. β-1,3 glucans are one such type of material that has exhibited diverse immunomodulatory effects on immune cells, including the mitigation or reversal of the adverse effects of dysregulated immune cells. In this review, we outline various fabrication techniques to produce β-1,3 glucan-derived microparticles and nanoparticles and discuss the diverse particle properties that can be obtained by tuning glucan chemistry, fabrication method, and formulation components. Furthermore, the immunomodulatory applications of β-1,3 glucan particles are highlighted with a focus on immune cell targeting, modulation, and the delivery of small molecule and macromolecular therapeutics.

1. Introduction

Many diseases, such as cancer and fibrotic diseases, involve the aberrant behavior of the body's own cells, particularly cells of the innate and adaptive immune system. For instance, macrophages (MΦ) play key roles in many pro- and anti-inflammatory processes including pathogen recognition and killing, phagocytosis of foreign particles, and injury resolution.[1] Due to this functional versatility, MΦ exhibits a wide range of properties that can be roughly divided into pro-inflammatory (M1-like) and anti-inflammatory (M2-like) phenotypes that exist on a spectrum that can be altered by various endogenous and exogenous stimuli. Similarly, dendritic cells (DCs) possess a diverse set of cell surface receptors for recognition and response to various stimuli. However, irregularly behaving immune cells contribute to poor or misaligned immune responses to diseases, such as overactive inflammatory responses or immunosuppression, that can significantly exacerbate both disease progression and severity. For example, one of the many ways cancerous cells avoid immune recognition is by releasing cytokines that inhibit the inflammatory responses and antigen-presenting abilities of innate cells like MΦ and DCs[2] while promoting local angiogenesis, tumor cell proliferation, and immunosuppression of the adaptive immune system.[3] Dysfunctional immune response is also a hallmark of progressive fibrotic diseases such as liver cirrhosis and pulmonary fibrosis, in which a chronic wound healing state (often resulting from repetitive tissue injury) is driven by pro-fibrotic MΦ that secrete cytokines that drive angiogenesis, fibroblast proliferation, and ultimately excessive extracellular matrix (ECM) deposition by myofibroblasts that alters tissue architecture and thus impedes organ function.[4] In all these cases, immune cells play an important role in both disease pathogenesis and progression and have thus become an important research area for developing novel and more effective therapeutics for immune-dysregulated diseases.

Traditional strategies to treat cancerous and fibrotic diseases have focused on the delivery of small molecule drugs designed to kill cells at the disease site and/or to inhibit one or more functions of the disease-progressing cells. Chemotherapy is one of the most commonly used cancer treatment methods in which potent cytotoxic drugs are delivered to the tumor to induce tumor cell death. However, most of these drugs do not possess cancer cell-specific cytotoxicity, and thus major systemic side effects are often induced due to the depletion of healthy cells in other tissues throughout the body. Similarly, in fibrotic diseases such as idiopathic pulmonary fibrosis (IPF), small molecule drugs such as nintedanib and pirfenidone have been shown to inhibit tyrosine kinase receptors on fibroblasts and MΦ in the lung, resulting in reduced ECM production and thus a slower rate of fibrotic progression.[5] However, these treatments also come with significant systemic side effects and are typically limited

N. Dowdall, T. Hoare
Department of Chemical Engineering
McMaster University
1280 Main St W, Hamilton, Ontario L8S 4L8, Canada
E-mail: hoaretr@mcmaster.ca

The ORCID identification number(s) for the author(s) of this article can be found under https://doi.org/10.1002/adhm.202501006

DOI: 10.1002/adhm.202501006

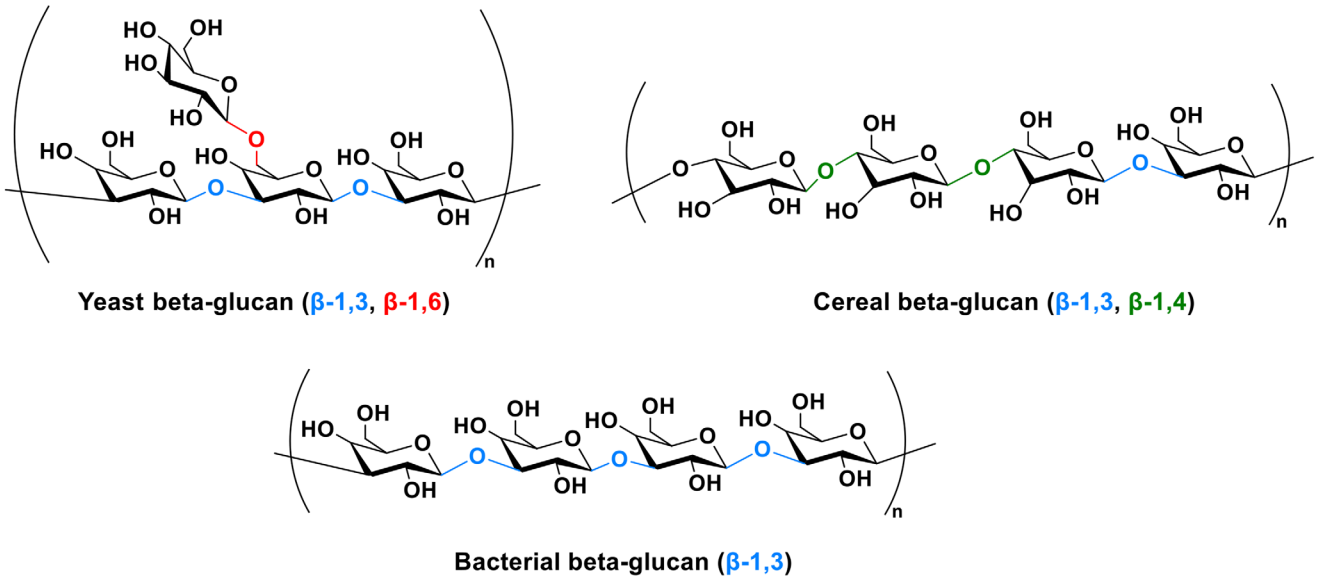

Figure 1. Chemical structures of BGs derived from various biological sources.

to only reducing the rate of fibrosis rather than preventing or reversing this process. As a result, there is currently a strong emphasis on developing alternative treatment methods with higher specificity and/or lower toxicity to both minimize side effects and improve treatment efficacy.

Immunomodulatory materials that are designed to target specific immune cells and alter their phenotype to achieve a desired function represent an emerging strategy to challenge and supplement or replace traditional therapeutic approaches.[6] By leveraging to the diverse range of cell surface receptors on immune cells, several natural and synthetic materials have been identified that can bind and activate one or more of these receptors to induce a desired cellular and thus immune response. Many of these receptors belong to the class known as pattern recognition receptors (PRRs), which evolved to identify specific pathogen-associated or damage-associated molecular patterns (PAMPs/DAMPs) expressed on pathogens or damaged cells, respectively.[7] Activation of these receptors can result in a myriad of cellular responses including the production of pro- or anti-inflammatory cytokines, the clearance of cellular debris, and/or the regulation of apoptosis.[7] Synthetic analogs as well as purified extracts of PAMPs/DAMPs have been developed that can effectively bind these receptors, thus opening the door to new material design strategies that can not only target immune cells but also modulate their behavior in a predicable fashion. One such material is β-1,3 glucan (BG), a polysaccharide PAMP expressed by several species of bacteria and fungi; several BG sources have been designated as Generally Recognized as Safe (GRAS) for food and beverage applications by the FDA.[8] BG binds the PRR Dectin-1 found on innate immune cells and, upon activation, induces a wide variety of immunomodulating responses that have sparked decades of research focused on harnessing these modulatory effects in applications ranging from vaccine development to targeted drug delivery. Indeed, several clinical trials have been conducted using various BGs for treating a broad range of indications including respiratory issues,[9] fatigue reduction,[10] vaccines,[11] and cancer therapy,[12] although there are currently no FDA-approved BG products available for biomedical applications. Furthermore, the immunomodulatory properties and appropriate application of BG-derived materials depend strongly on many material design parameters such as particle size, morphology, and surface chemistry that are critical to understand and thus engineer to promote the desired immune response with the desired specificity to optimize disease treatment. For example, soluble β-1,3 glucans, while capable of binding Dectin-1, induce poor Dectin-1 signaling[13] or no signaling at all[14] depending on molecular weight and chain conformation[15]; conversely, particulate β-1,3 glucans are typically strong inducers of Dectin-1 signaling, although both binding affinity and downstream biological effects depend strongly on particle purity and particle size. As such, rational engineering of BG-based micro/nanoparticles is essential to leverage the immunomodulatory potential of BG for practical clinical applications.

In this review, we discuss the potential of utilizing β-1,3 glucans in microparticle or nanoparticle form as a therapeutic to modulate innate immune cells like MΦ and DCs. We specifically focus on the various fabrication methods to prepare BG-derived particles (both on the micro and nanoscale), their physicochemical and immunomodulatory properties, and the major applications associated with these materials.

2. Beta-Glucans as Immunomodulatory Materials

BGs are a class of glucose homopolymers linked by β-1,3, β-1,4, or β-1,6 glycosidic bonds or combinations thereof that are found in a wide variety of natural sources including bacteria, fungi, and cereals like oats and barley. The chemical structures of some common BGs are shown in **Figure 1**. BGs typically function as structural components in cereals and fungi and as storage polysaccharides in various bacteria.[16] Depending on the source, BGs can vary widely in their physicochemical properties. Oat and barley BGs are linear polysaccharides comprised of a combination of

β-1,3 and β-1,4 linkages with molecular weights (MWs) ranging from tens of thousands to millions of Daltons[17] and are typically water soluble, forming viscous solutions or even gels depending on their concentration, molecular weight, and the ratio of β-1,3 to β-1,4 linkages.[17] Linear BGs are also produced by bacteria, the most common being curdlan which is produced by various bacterial genera including *Agrobacterium* and *Rhizobium*.[18] Similar to cereal-derived BGs, the molecular weight of curdlan can vary widely; however, since it is composed entirely of β-1,3 linkages, curdlan produces single and triple helical structures in aqueous solutions that introduce thermoresponsive gelation properties.[18] Conversely, the BGs produced by fungi like yeast and mushrooms typically consist of a β-1,3 linked backbone with β-1,6 linked sidechains and comprise up to 90% of all glucans in the fungal cell wall[19] and ≈50% of the cell wall by mass,[20] making them one of the cell wall's major structural components. Fungal BGs are high molecular weight polysaccharides (ranging from hundreds of thousands to millions of Daltons)[19,21] that adopt triple helical structures in solution via strong hydrogen bonding, resulting in water-insoluble supramolecular structures that can be denatured via heat, alkaline pH, or some organic solvents like DMSO.[22] Due to the wide range of physicochemical properties accessible between different types of BGs, their use has been explored in several areas including food, cosmetics, veterinary medicine, and pharmaceutical/nutraceutical applications.[23]

While a variety of β-glucans have been reported to exhibit at least weak immunomodulatory properties, β-1,3 glucans from fungal and bacterial sources have been demonstrated to induce particularly strong immunomodulatory effects and thus have been researched for this purpose over several decades. Zymosan, a crude yeast cell wall extract containing various polysaccharides and proteins, was first reported in the 1940s and subsequently studied for its ability to induce immune responses like increased pro-inflammatory cytokine production[21,24]; it was not discovered until the 1970s that β-1,3 glucan was the component responsible for such immunomodulatory effects. Subsequent efforts were focused on isolating β-1,3 glucans from several fungal sources, including lentinan (a β-1,3/1,6 glucan from *Lentinus edodes*)[25] and schizophyllan (a β-1,3/1,6 glucan from *Schizophyllum commune*),[26] that yielded better-defined properties while limiting the intensity of the inflammatory response associated with Zymosan.[27]

The mechanism behind the immunomodulatory properties of such β-1,3 glucans was clarified in 2001 when Brown and Gordon identified Dectin-1 (a receptor that was initially discovered on DCs)[28] as a β-1,3 glucan-specific cell surface receptor on MΦ,[29] leading to extensive subsequent attention on the use of beta-glucans as Dectin-1 binding (and thus MΦ- and DC-targeting) materials. In macrophages, the activation of Dectin-1 can induce phagocytosis as well as the production of a range of pro-inflammatory cytokines including tumor necrosis factor-alpha (TNF-α), IL-6, and IL-23[30] accompanied by a decrease in common M2 markers such as arginase, CD206, and transforming growth factor beta (TGF-β);[31] as such, Dectin-1-activated MΦ typically adopt a pro-inflammatory M1-like phenotype. Several studies have shown that Dectin-1 activation via beta-glucan can induce repolarization of an M2-like MΦ to an M1-like phenotype.[32] For instance, Liu et al. showed that bone marrow-derived MΦ polarized to the M2-like phenotype could be repolarized to M1-like via treatment with particulate yeast beta-glucan (YBG, which is rich in β-1,3 glucan) in a Dectin-1-dependent manner,[32a] inducing significant increases in several M1 markers like iNOS, IL-12, TNF-α, and IL-1β with a simultaneous reduction in M2 markers like IL-10 and arginase. Correspondingly, de Graff et al. showed that YBG as well as other β-1,3 glucans like Zymosan and curdlan could induce the secretion of IL-6, TNF-α, and IL-10 from human MΦ while also significantly increasing the expression of chemoattractants involved in monocyte recruitment and activation.[32c] Similarly, β-1,3 glucan binding to DCs can lead to a myriad of immunological responses at both the innate and adaptive levels. For instance, orally administered YBG particles can be taken up by DCs in tumor-bearing mice, resulting in upregulation of DC surface markers, increased DC and T cell tumor infiltration, and signification modulation of the cytokine profile in the tumor microenvironment (TME).[33] Bone marrow-derived DCs (BMDCs) treated with YBG have also been shown to upregulate the production of pro-inflammatory cytokines and markers such as TNF-α and iNOS.[34] As such, β-1,3 glucans can effectively modulate the behavior of any immune cell in which Dectin-1 is expressed.

As the immunomodulatory properties of β-1,3 glucans continue to be elucidated, several unique beta-glucan-based formulations have been developed to address a diverse range of immunological diseases/disorders. In the following sections, we will describe various beta-glucan micro/nanoparticle preparation techniques, their potential advantages/disadvantages, and their corresponding applications in the context of immunomodulation and/or the targeted delivery of therapeutics.

3. Beta-Glucan Microparticles

Microparticles possess several advantages in the context of immunomodulation. Micron-sized particles, especially those in the single micron diameter range, are optimally sized for phagocytosis by cells like MΦ and DCs,[35] with phagocytosis further promoted by Dectin-1 mediated binding to BG. Such enhanced phagocytosis may be desirable for drug-loaded microparticles in which intracellular drug delivery is required, such as the delivery of drugs to *M. tuberculosis*-infected MΦ.[36] Microparticles also have the potential for higher drug content per particle compared to nanoparticles (NPs); furthermore, due to their smaller surface area-to-volume ratios, microparticles often experience less drastic burst drug release.[37] Finally, microparticles are highly desirable in applications requiring inhaled administration, with smaller microparticles (typically in the 1–5 µm range) in particular offering an optimal balance between effective inhalation and subsequent deposition in the lower airways where many diseases like tuberculosis and pulmonary fibrosis occur.[38]

While microparticle preparations from other sources such as curdlan[39] and mushroom BGs[40] have been reported, the vast majority of the literature describes the preparation of yeast-derived beta-glucan (YBG) microparticles; as such, we will confine our scope of discussion around BG-based microparticles to YBG preparations and their corresponding physicochemical and immunomodulatory properties.

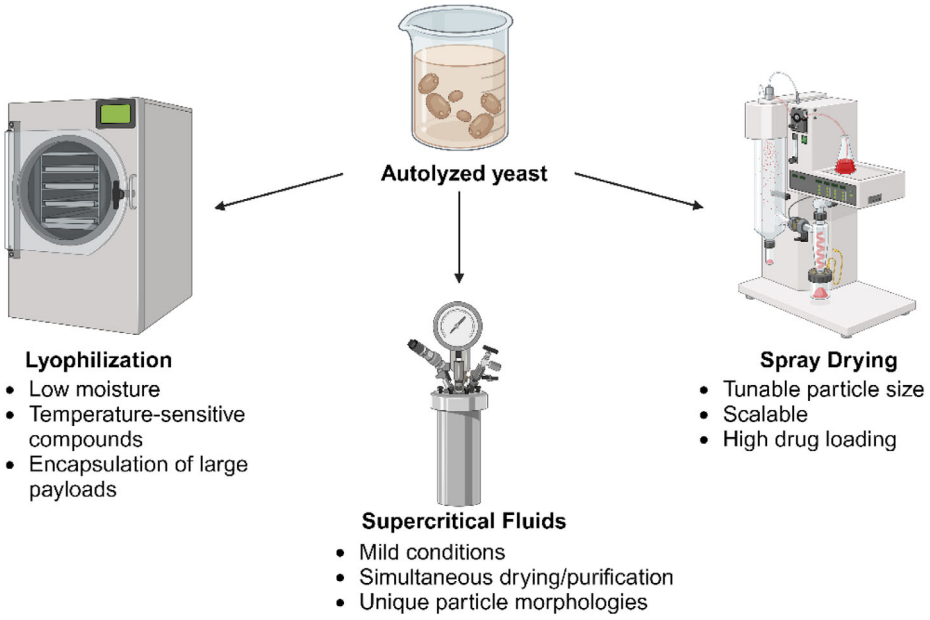

Figure 2. Common processing techniques to prepare YBG microparticles. Created with BioRender.com.

3.1. Preparation of Yeast-Derived Beta-Glucan (YBG) Microparticles

Since β-1,3/β-1,6 glucan comprises a large fraction of the cell wall of yeasts such as *S. cerevisiae*, isolation of beta-glucan from intracellular components results in the formation of hollow microparticles, often described as "yeast ghost cells".[30b,41] The most common method to prepare YBG is to subject yeast cells to a series of alkaline and acidic extractions, with the combination of altered pH and elevated temperatures inducing cell autolysis and thus the degradation of proteins, nucleic acids, and phospholipids both in the cytoplasm and within the cell wall.[42] The crude insoluble product is then washed several times with various solvents to remove residual soluble material, after which the purified slurry is dried to a fine powder consisting of the hollow YBG microparticles. A typical protocol is outlined by Hromádková et al., in which they prepared YBG through sequential NaOH extractions with various temperatures (60–90 °C) and NaOH concentrations (3%–6%).[43] After removing the soluble impurities, the insoluble material was further extracted in 4% phosphoric acid followed by several washes with water and oven dried to remove residual moisture. Depending on the cell strain and extraction parameters, the final protein content of YBG can range from 1%–20%, and the total carbohydrate content can range from ≈50 to > 90%.[32c,43,44] However, the final particle properties, such as size, morphology, and ultimately immunomodulatory activity, largely depend on the final drying step, the methods for which are schematically depicted in **Figure 2** and further outlined in the subsequent section.

3.1.1. Solvent Evaporation

Solvent evaporation is one of the most common YBG drying techniques in which a cake of YBG in residual solvent (typically water, ethanol, or acetone) is left to dry under either ambient, oven, or vacuum conditions.[43,44b,45] Air drying has the obvious benefit of low cost and simple setup but is limited by longer drying times and its scalability to larger batch sizes. Another disadvantage of air drying is the tendency of particles to aggregate during drying via capillary forces, often yielding particle sizes in the 100–500 µm range[45a,b] that are too large for MΦ phagocytosis and thus require subsequent processing methods (e.g., mechanical grinding) to reduce the particle size. However, such mechanical de-aggregation processes can often result in very broad particle size distributions, with one such study reporting that only 10% of the particle distribution was below 10 µm[45c] (the target size range for effective MΦ uptake).[46] Grinding and other mechanical processes can also lead to inconsistent and nonuniform particle morphologies that may lead to unpredictable recognition and uptake by innate immune cells. While some studies have shown the ability to prepare sub-10 µm YBG particles via air drying,[47] these methodologies typically require the use of highly volatile solvents like acetone during the drying step and/or differences in the time or intensity of the extraction steps that can pose further scalability challenges.

Improved control over YBG particle properties can be achieved through spray drying, in which a feed solution or suspension is passed through an atomizer to generate fine droplets from which the solvent is rapidly evaporated in a high-temperature drying chamber under constant hot air flow. The dried particles are then transported to a collection jar via centrifugal forces, filter bags/membranes, or electrostatic deposition.[48] Spray drying possesses several advantages over air drying: 1) atomization of the feed solution greatly increases the interfacial surface area, promoting rapid drying through improved heat/mass transfer rates; 2) adjusting the size of the atomized droplets allows for tunability of the final dried particle size; and 3) spray drying technology is significantly more scalable, allowing for microparticle production on both the lab scale (milligrams to kilograms per day)

and industrial scale (several tons per day).[49] Improved control over particle size can also be imparted by adjusting the droplet size (and thus the average number of particles contained in a droplet) based on the inlet flow rate, inlet temperature, drying gas flow rate, atomizer type, and solvent vapor pressure,[49a] in some cases enabling the preservation of the original size of the autolyzed yeast cells.[47b,50] In general, the feed flow and atomizer rates should be optimized for small droplet sizes to minimize the number of particles per droplet, thus preventing the aggregation of adjacent particles during droplet drying. Other parameters like high temperatures and/or low boiling point solvents can increase the evaporation rate and minimize residual moisture, which can further prevent subsequent particle aggregation and increase shelf life. YBG microparticles in the 1–10 μm range have been demonstrated to be prepared over a range of spray dryer parameters, typically using inlet temperatures = 110–180 °C, outlet temperatures = 45–120 °C, liquid flow rates = 0.25–0.3 L h^{-1}, and gas flow rates = 246–700 L h^{-1}.[44,45b,c,47b,50,51]

The differences in YBG properties achieved between the air drying and spray drying techniques were well illustrated by Petravić-Tominac et al., who assessed the effects of both the extraction process and drying method on the purity and size of YBG particles from spent brewer's yeast. When alkaline/acidic extractions were combined with an additional mannoprotein removal step, the spray-dried product consisted of approximately 4% proteins, 95% β-glucan, and a median particle size of 6.6 μm[45a]; in contrast, while the air-dried analog showed similar purities, the particle size distribution consisted of large aggregates with a median size of 266 μm that needed to be broken up by sonication into more irregular particles as small as 1–2 μm that do not significantly aggregate upon resuspension in water.[44b] Similar results were reported by Ruphuy et al., who showed the potential of ultrasonication to produce stable dispersions (mean size ≈5 μm) of both air-dried and spray-dried YBG.[47b]

In addition to improved control over particle size, spray drying offers the ability to prepare drug-encapsulated YBG microparticles, sometimes in a single processing step. Due to its porous shell and hollow interior, YBG can encapsulate a variety of payloads at high loadings. Typically, YBG is suspended in a solution containing the desired drug for a pre-determined time period, after which the YBG/drug mixture is spray-dried to form a fine powder. As the atomized droplets evaporate, drug molecules become confined and ultimately precipitate in the hollow YBG cavity or on the highly porous YBG surface, resulting in simultaneously dried and drug-impregnated YBG composites that can be designed to exhibit high drug loading efficiencies.[47b,52] For example, Dadkhodazade et al. prepared cholecalciferol-loaded YBG via diffusion-based loading followed by spray drying. The drug-loaded particles had an encapsulation efficiency (EE%) of 76% while exhibiting a slightly increased mean particle size compared to unloaded YBG (4.5 vs 3.4 μm, respectively).[53] Ahmad et al. analogously demonstrated that spray-drying drug-loaded YBG can yield small geometric and aerodynamic diameters (1–6 μm and 1–2 μm, respectively), suggesting that YBG can be effectively inhaled for the delivery of pulmonary therapeutics.[54] Other studies have shown that spray drying YBG in the presence of a drug can achieve drug contents as high as 20 wt.%,[50] with EE% sometimes in excess of 95% upon optimization of the drug concentration in the feed.[51] Beyond the high EE% achievable, spray drying can also offer the advantage of encapsulating drugs in the amorphous state even at high drug loadings, which is highly desirable for pharmaceutical formulations given that amorphous solid dispersions often exhibit increased dissolution rates and thus higher bioavailable drug concentrations compared to their crystalline counterparts.[50] For example, curcumin loaded on YBG by spray drying was found to exist entirely in the amorphous state at target loadings up to 20 wt.%, resulting in an initial dissolution rate four times greater than that achieved with a physical mixture of YBG and curcumin.[50] Spray drying can thus provide more scalable preparation of both pure and drug-loaded YBG microparticles with superior particle size control over other evaporative processes.

3.1.2. Lyophilization

Lyophilization, or freeze drying, is the process of removing water from a frozen sample via sublimation in a high vacuum environment, with the resulting vapor condensed on low-temperature (−40 to −80 °C) coils in a collection chamber. Lyophilization is an important unit operation in both the food and pharmaceutical industries to prepare powdered materials with low moisture content[55] and has also been widely used to prepare both pure and drug-loaded YBG materials. While lyophilization often requires less process optimization compared to spray drying, lyophilization can lead to YBG deformation. For example, in a study by Zechner-Krpan et al., lyophilization yielded smaller YBG particles (4.0 μm median diameter) compared to spray-dried YBG (6.6 μm median diameter) but resulted in irregular porous agglomerates of beta-glucan particles while spray drying better preserved the yeast cell morphology.[45b] Other studies have shown that these freeze-dried agglomerates can be broken up into individual YBG particles (≈2–3 μm) through additional probe sonication treatment,[56] although this represents an additional step that is challenging to scale.

Despite these drawbacks, lyophilization is most frequently used as the final drying step to prepare drug-,[36b,51,57] protein/peptide-,[58] or NP-[59] loaded YBG composites by taking advantage of the porous glucan shell; however, rapid release of in particular small molecule drug payloads typically occurs for the same reason unless these pores are sufficiently sealed. For example, Soto et al. loaded the tuberculosis drug rifampicin into YBG microparticles by swelling the YBG in a solution of rifampicin, performing a pH-induced precipitation of the drug inside the YBG core, and drying via lyophilization.[36b] While drug loading contents of >30 wt.% were achieved, rapid burst release of nearly 100% release within one hour was observed unless the YBG was encapsulated within a lyophilized alginate/chitosan hydrogel shell to extend drug release by several hours. A similar result was observed by Lee et al., in which YBG was loaded with the cancer therapeutic doxorubicin (DOX), sealed inside an alginate/chitosan polyelectrolyte layer, and lyophilized to remove water.[57a] The composites had a particle size of 3–5 μm, a drug loading content of 1.05 wt.%, an EE% of 52%, and enabled DOX release for >48 h, significantly longer than the unencapsulated YBG particles (90% release after 24 h). The encapsulation of larger payloads such as proteins, quantum dots, and NPs into YBG alternately offers a "nano-in-micro" approach to address

issues such as burst release, inefficient targeting, or unstable payloads. To achieve high loadings, aqueous mixtures of drug payload and YBG are most commonly subjected to a series of hydration/lyophilization cycles through which capillary forces push the payload through the porous YBG shell and into the hollow core.[59a,d,g] Soto et al. were the first to demonstrate this approach by loading 20 nm polystyrene NPs into YBG using two hydration/lyophilization cycles (resulting in an EE% of >80%);[59a] the same group achieved similar results with precipitated gallium NPs (EE% > 65%).[59b] While this group suggested that YBG's pore size of approximately 40 nm would inhibit the loading of larger payloads,[59a] successful loading of NPs with a range of diameters has now been demonstrated into YBG. For instance, Ren et al. successfully loaded 68 nm polymer/lipid hybrid NPs into YBG with an EE% of 46%,[59d] a process driven by both capillary action from the hydration/lyophilization cycles and the electrostatic interactions between the cationic NPs and the slightly anionic YBG. Similar encapsulation efficiencies were reported with drug-loaded poly(lactic-co-glycolic acid) (PLGA) NPs with a diameter of 92 nm,[59g] while Zhou et al. used confocal microscopy to show that polystyrene NPs as large as 750 nm could be encapsulated in the YBG core.[59c] However, to achieve the loading of such larger particles, NPs with high positive surface charges appear to be required to supplement the capillary force-induced loading. Furthermore, there are discrepancies in the literature regarding the pore size of YBG, with some estimates suggesting the porosity is as high as 600 nm.[60] It is likely that the YBG pore size will vary significantly depending on both the extraction method used (i.e., the extent of cell wall hydrolysis) and the drying method used (potential pore collapse during evaporative/sublimation processes). However, despite the importance of the YBG pore size to the practical use of YBG, the pore size is rarely reported in the literature; as such, more detailed investigations into the surface properties of YBG thus offer promise to better design encapsulation strategies for loading payloads of various sizes.

3.1.3. Supercritical Fluids

While solvent evaporation and lyophilization represent the most popular processing/drying methods for YBG, the use of supercritical fluids to process YBG has recently gained interest given its potential to avoid some of the drawbacks of sublimation and evaporative processes. Supercritical CO_2 ($scCO_2$), the most commonly used supercritical processing fluid, presents several advantages in material processing: 1) CO_2 becomes supercritical at relatively mild conditions (31 °C and 7.4 MPa),[61] allowing for the stable processing of thermosensitive materials and therapeutics; 2) supercritical fluids possess properties intermediate of liquids and gases, exhibiting gas-like diffusivity and liquid-like solvating power[62] that allows for the solvation of a wide range of therapeutics and efficient penetration of the fluid into microparticles; 3) the absence of an air-liquid interface results in a more gentle drying process via solvent extraction that can preserve fine morphologies and avoid drying artifacts commonly associated with evaporation/lyophilization; and 4) supercritical fluids may extract various small molecule and macromolecular impurities that would otherwise be enriched on the particle/material surface during evaporative and sublimation processes and may compromise receptor affinity.[63] While the supercritical processing of polysaccharides (including the extraction of various beta-glucans) via supercritical fluids is well documented,[64] demonstration of the processing of YBG is relatively recent. For example, $scCO_2$ was used to prepare both barley and yeast beta-glucan aerogels by first preparing alcogels from the polysaccharides and then removing the solvent in a critical point dryer,[65] yielding a highly porous YBG matrix with a specific surface area as high as 178 $m^2\ g^{-1}$. Acetylsalicylic acid could then be loaded into these high surface area aerogels using a supercritical impregnation process to achieve drug loading capacities of up to 15 wt.%,[65] albeit with a significant alteration in the YBG particle size and morphology leading to the generation of aggregated/fused YBG particles. Such dramatic alterations of YBG's original physical properties may negatively affect its ability to exert immunomodulatory effects, although such an impact was not specifically investigated. As an alternative, Errenst, Petermann, and Kilzer reported the encapsulation of limonene into spent yeast cells using the concentrated powder form (CPF) process, which involves the rapid mixing of a powder with a mixture of a supercritical fluid and a liquid.[66] Fluidized yeast cells were injected into a spray tower through one nozzle, while a mixture of $scCO_2$ and a limonene/water emulsion was atomized through a separate nozzle. The rapid mixing of these streams resulted in the deposition of limonene on the yeast cell wall and (after storage times of 2–168 h) the diffusion of limonene inside the cells, resulting in limonene loadings of up to 20 wt.% with no major alterations to YBG morphology;[66] however, large agglomerates of individual yeast cells were observed and the ability to redisperse these cells was not investigated. Furthermore, it is important to note that intact spent yeast cells were used in this work, likely resulting in significantly different physical and biological properties compared to pure YBG including diminished Dectin-1 interactions or other potentially undesirable effects such as Toll-like receptor activation.[60] However, due to its high drug loading capacity and preservation of surface morphology, the CPF method offers the potential to efficiently load YBG microparticles with a wide range of liquid payloads.

Recently, our group first demonstrated a supercritical fluids-based processing strategy for YBG that preserved the discrete size and morphology of individual YBG microparticles using Pressurized Gas eXpanded liquids technology (PGX^{TEC}).[67] The PGX^{TEC} process uses a mixture of $scCO_2$ and ethanol that, when co-injected into a pressurized vessel with an autolyzed yeast slurry, rapidly removes solvents and other impurities from the slurry, resulting in dried, highly uniform YBG particles. The presence of ethanol in the PGX^{TEC} fluid is crucial for the processing of aqueous formulations given that it promotes miscibility between the aqueous input stream and the PGX^{TEC} fluids as well as simultaneously processes and dries an effectively sterile material.[64d] PGX^{TEC}-processed YBG (PGX^{TEC}-YBG) presents a desirable set of properties such as small size (≈5 µm with narrow size distributions), significantly higher specific surface areas compared to spray-dried YBG analogs (> 130 $m^2\ g^{-1}$ compared to < 5 $m^2\ g^{-1}$ for spray dried YBG), and extremely low bulk densities as low as 0.05 g mL^{-1} (**Figure 3**).[67] PGX^{TEC}-YBG also exhibits a higher surface purity compared to spray-dried YBG, potentially contributing to the observed

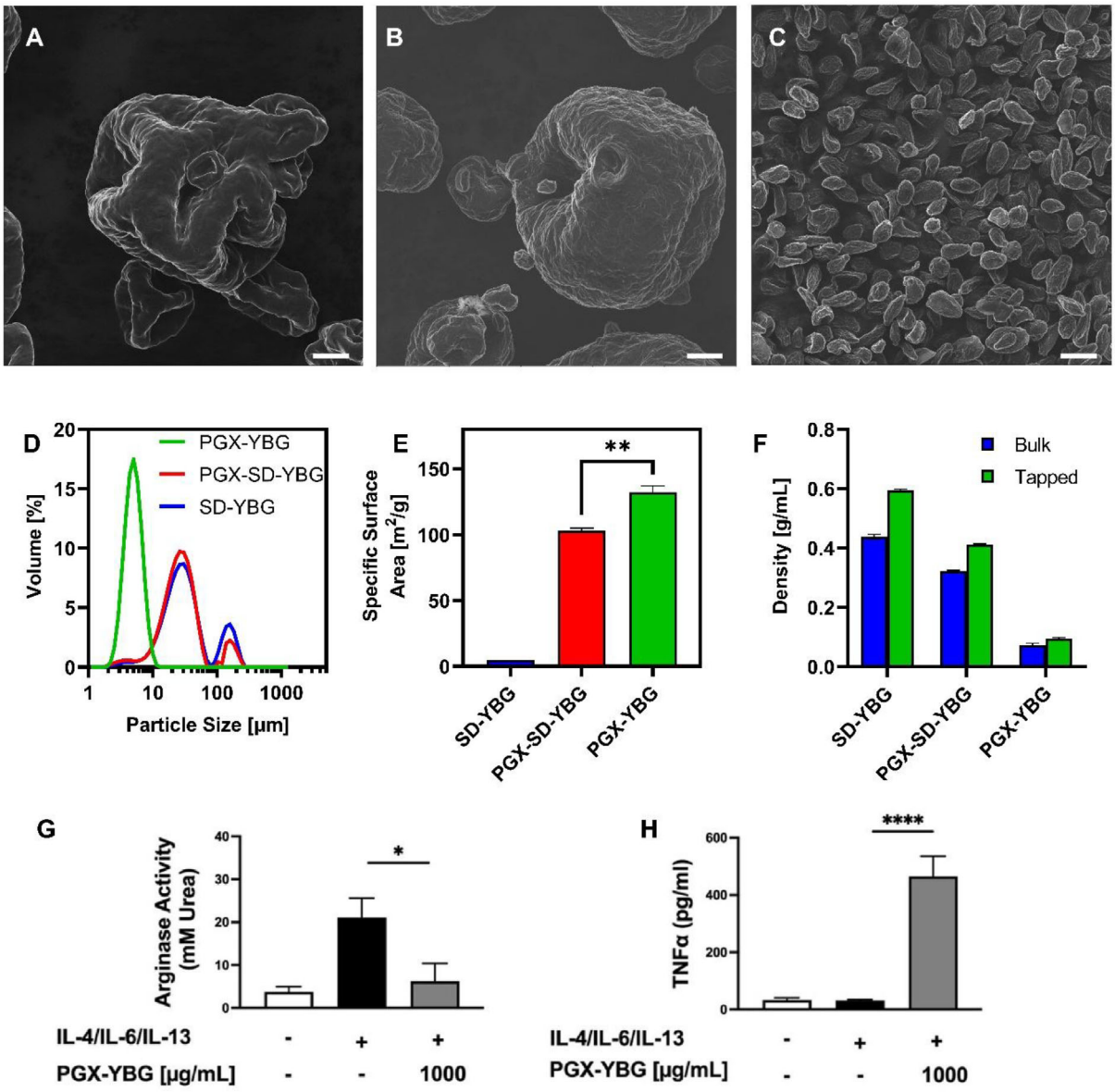

Figure 3. Physical, morphological, and immunomodulatory characteristics of spray-dried and PGX^{TEC}-processed YBG powders highlighting the importance of the processing method on the physicochemical and immunomodulatory properties of YBG. A–C) Helium ion microscopy images of (A) spray-dried YBG (SD-YBG), (B) PGX^{TEC}-processed SD-YBG (PGX-SD-YBG), and (C) PGX^{TEC}-processed YBG (PGX^{TEC}-YBG); scale bars = 5 μm; D–F) Comparison of particle size (D), specific surface area (E), and density (F) between YBG powders processed using different methods, showing the benefits of the PGX^{TEC} process in creating smaller and highly porous microparticles; G, H) Immunomodulatory activity of PGX-YBG in murine precision cut lung slices, illustrating PGX^{TEC}-YBG's ability to modulate both M1 (TNF-α) and M2 (arginase) macrophage markers. Adapted with permission.[67] Copyright 2025, Elsevier.

higher surface porosity and enhanced Dectin-1 activation in vitro.

3.2. Immunomodulatory Applications of β-1,3 Glucan Microparticles

3.2.1. Stand-Alone Innate Immune Cell Modulators

Due to β-1,3 glucan's inherent immunomodulatory properties, YBG microparticles have been investigated as standalone therapeutics to modulate immune cell behavior. A summary of YBG's immunomodulatory applications is presented in **Table 1**. YBG alone is readily phagocytosed by DCs in vitro and stimulates TNF-α secretion in a Dectin-1-dependent manner.[68] YBG also targets and activates DCs in vivo, which can promote DC and T cell tumor infiltration and subsequent tumor regression.[33] Importantly, these effects can be achieved via oral delivery, which is desirable for ease of administration and patient compliance. YBG has also been reported to exert immunological changes in MΦ via several mechanisms including altered gene expression, inflammatory cytokine upregulation,

Table 1. Summary of papers highlighting the immunomodulatory applications of YBG microparticles.

YBG Preparation Method	Size	Other Components/ Therapeutics	Drug Loading	Application	Main Immunomodulatory Outcomes	Ref.
Air drying	2–4 µm	N/A	N/A	DC modulation	Stimulated TNF-α secretion in BMDCs; synergistic activity with TLR agonists.	[68,74]
Lyophilization	Not specified	N/A	N/A	Trained immunity against *M. tuberculosis* infection	BG-trained mice showed enhanced response to infection, greatly improving survival rates	[73,75]
Not specified	4–6 µm	N/A	N/A	DC modulation in tumor-bearing mice	Enhanced T cell/DC activation/infiltration; reduced tumor growth	[33,76]
Not specified	4–6 µm	N/A	N/A	MΦ modulation in tumor-bearing mice	Significant increase in M1/M2 marker ratio; reduced tumor volume in vivo	[32a,76]
Not specified	4–6 µm	N/A	N/A	MΦ modulation in tumor-bearing mice	Reduced tumor growth due to enhanced M1 MΦ and NK cell tumor infiltration	[69,76]
Not specified	4–6 µm	N/A	N/A	Trained immunity in murine TAMs	BG-trained MΦ resulted in metastasis inhibition, improved survival rates	[72b,76]
PGX^{TEC} processing	5 µm	N/A	N/A	Modulation of pro-fibrotic lung MΦ	Significant reduction in arginase; increased TNF-α production in murine ex vivo lung tissues	[67]
Not specified	Not specified	N/A	N/A	Reprogrammed human TAM-like MΦ in vitro	Increased secretion of M1 cytokines and chemoattractants	[32c]
Not specified	Not specified	N/A	N/A	Trained immunity in human monocytes	Enhanced TNF-α and IL-6 production after LPS challenge	[72a]
Air drying	2–4 µm	Encapsulated AS04 adjuvant and *T. gondii* lysate	EE% ≈40% LC% ≈4%	Vaccine adjuvant	Improved uptake, lymph node accumulation, and survival in infected mice	[77]
Lyophilization	Not specified	Encapsulated ovalbumin/tRNA complexes	EE% > 90%	Vaccine adjuvant	Enhanced T cell proliferation and Th1/Th17 responses in vaccinated mice	[58b,78]
Not specified	≈1.7 µm	Surface conjugated NY-ESO-1 antigen	5–7.5 × 10^5 antigen molecules per yeast cell	Vaccine adjuvant	Effective cross-presentation and immunization of T cells in vitro	[79]
Vacuum drying	Not specified	Surface conjugated ovalbumin	LC%; 1%	Vaccine adjuvant	Activation and proliferation of CD4+/CD8+ T cells in vitro	[44b,80]
Air drying	2–6 µm	Encapsulated bovine serum albumin and surface conjugated aminopeptidase N antibody	EE% ≈97% (both bovine serum albumin & aminopeptidase N)	Vaccine with aminopeptidase N-targeting	Improved IgG titres in pigs compared to free antigen	[58b,81]
Not specified	Not specified	Conjugated adenovirus	Not specified	TAM modulation	Strong modulation of cytokines, metabolites, MΦ phenotype in vivo	[82]
Lyophilization	≈3 µm	Encapsulated berberine (BBR)/epigallocatechin gallate (EGCG) NPs	EE% ≈60% (BBR), 93% (ECGC)	Colon-targeted drug delivery	Significant reduction in colon inflammation and M1 cytokines in vivo	[83]
Air drying (pure); lyophilization (loaded)	≈2–4 µm	Encapsulated cabazitaxel-loaded polymer/lipid NPs	EE% = 45.6% LC% = 1.8%	MΦ-targeted oral delivery	Improved bioavailability of cabazitaxel in vivo	[59d]

(*Continued*)

Table 1. (Continued)

YBG Preparation Method	Size	Other Components/ Therapeutics	Drug Loading	Application	Main Immunomodulatory Outcomes	Ref.
Air drying	≈2–4 µm	Encapsulated DNA/tRNA/poly-ethyleneimine polyelectrolyte complexes	~ 10^6 DNA molecules/particle	Targeted gene delivery	Improved transfection of Dectin-1-expressing cells compared to DNA/poly-ethyleneimine NPs	[81b]
Not specified	≈4–5.5 µm	Encapsulated doxorubicin	EE% = 62.7% LC% = 11.4%	Tumor-targeted drug delivery	Accumulation in TAMs; retention in murine tumors over 7 days	[84]
Lyophilization	3–5 µm	Encapsulated doxorubicin; chitosan/alginate surface coating	EE% = 52.4% LC% = 1.1%	Controlled drug release system	Significant TNF-α and IL-2 secretion in PBMCs	[57a]
Vacuum drying (pure); Lyophilization (loaded)	≈2–4 µm	Encapsulated methotrexate immobilized in alginate hydrogel	EE% ≈85% LC% ≈17%	Colon-targeted drug delivery	Targeted delivery to intestinal MΦ; reduction in colitis symptoms in mice	[57c]
Lyophilization	≈3 µm	Q11 peptide-based hydrogel encapsulated in YBG cavity	LC% = 2.1%–2.3%	MΦ-targeted oral delivery	Higher Dectin-1-mediated MΦ uptake in vivo compared to peptide alone	[58a]
Vacuum drying (pure); lyophilization (loaded)	≈2–8 µm (loaded)	Encapsulated various NPs, small molecule drugs	LC% ≈7–56%	MΦ-targeted inflammation/cancer therapy	Reduction in local inflammation or tumor burden in various in vivo models	[59c]
Lyophilization (pure); Slurry evaporation, spray drying (loaded)	Not specified	Various encapsulated anti-inflammatory compounds	LC% ≈0.02%–0.05%	MΦ-targeted drug delivery	Enhanced suppression of NF-κB and ROS in vitro compared to free drug	[51]
Lyophilization	2–4 µm	Emodin/asiatic acid encapsulated in YBG; chitosan/alginate microgel encapsulating YBG and *L. casei* Zhang	EE% = 75%–90% LC% = 20%–60%	Renal fibrosis therapy	Significantly reduced fibrosis; improved gut microbiota diversity in vivo	[85]

as well as the production of chemoattractants responsible for monocyte and neutrophil recruitment.[32c] In cancer models, these immunomodulatory properties have been shown to "re-program" tumor-associated MΦ (TAMs) to a pro-inflammatory phenotype that not only upregulates M1 markers like iNOS, IL-12, and TNF-α but also downregulates IL-10, arginase, and other M2 markers.[32a] YBG-induced TAM reprogramming has thus shown promise as an alternative cancer treatment method, demonstrating reduced tumor growth in multiple murine cancer models.[32a,69]

We recently showed that YBG's immunomodulatory activity extends to MΦ involved in fibrotic lung disease using three different cell lines: human THP-1 MΦ, murine bone marrow-derived macrophages (BMDMs), and murine alveolar MΦ. PGX^{TEC}-processed YBG can effectively downregulate M2 markers associated with lung fibrosis including arginase and CCL18 while subsequently upregulating the M1 marker TNF-α, albeit not to an extreme polarization state that would induce an undesirable inflammatory response. Such effects were demonstrated in a pre-polarized in vitro model (in which MΦ were first polarized to an M2-like phenotype followed by PGX^{TEC}-YBG treatment), a co-polarized in vitro model (in which the M2 cytokines and PGX^{TEC}-YBG were administered simultaneously), and a murine precision-cut lung slice (PCLS) ex vivo model (which better replicates the complex cellular processes and lung architecture seen in vivo, Figure 3G,H). The capacity of PGX^{TEC}-YBG to prevent the M2-polarization of naïve MΦ is particularly relevant for lung fibrosis in which infiltrating monocytes are polarized to an M2-like phenotype upon reaching the lung to contribute to the fibrotic milieu.[70]

In addition to modulating immune cells in diseased tissues, recent studies have highlighted the potential for β-1,3 glucans to induce trained immunity, a recently discovered phenomenon that confers a nonspecific memory to innate immune cells in response to immunomodulatory stimuli via metabolic and epigenetic reprogramming.[71] Leveraging materials that induce trained immunity has implications in a variety of applications, including improved cancer and vaccine therapies.[71b] Multiple in vitro models have shown that pre-treating (i.e., training) MΦ with YBG results in stronger pro-inflammatory responses to LPS challenge compared to both negative controls and soluble BG.[72] Ding et al. further explored YBG-induced trained immunity in vivo by injecting YBG-trained mice with tumor cells to assess the effects of YBG training on tumor burden. Trained mice showed markedly fewer tumor nodules in the lungs and significantly higher survival rates compared to control mice, with a 60% survival rate achieved after 60 days.[72b]** YBG training also shows benefits in tuberculosis treatment, with mice trained using YBG achieving an 80% survival rate 300 days after *M. tuberculosis* infection.[73] While Dectin-1 is presumed to play a major role in YBG-induced immunity, the resistance response was found to heavily rely on IL-1 signaling,[73] potentially indicating another therapeutic target for inducing trained immunity.

While many papers have published similar overall trends associated with immunomodulatory properties of YBG, as Table 1 shows many papers do not specify the processing method used

and/or the size of the YBG being studied. As such, the capacity to draw rigorous structure-property correlations from the literature is unfortunately limited. Given the strong correlation between YBG size, aggregation state, porosity, purity, and immune cell interactions/responses, we would suggest that information on processing method, size, and aggregation state is essential in any future publication in this area.

3.2.2. Vaccine Formulation

The ability of β-1,3 glucan microparticles to target and modulate antigen-presenting cells (APCs) like DCs and MΦ makes it an ideal carrier and adjuvant for vaccine formulations that heighten the corresponding immune response.[86] While traditional adjuvants have been based around aluminum salts and oil-in-water emulsions,[86a] there has been increasing research exploring the use of β-1,3 glucans as naturally derived alternatives that avoid many of the formulation and tissue compatibility challenges of other options. In this context, YBG can enhance each cell targeting, payload encapsulation/conjugation, and adjuvanticity beneficial to effective vaccination. Huang et al. compared the vaccination efficacy of ovalbumin (OVA)-loaded YBG microparticles and OVA-complexed alum using in vitro, in vivo, ex vivo models[78] and reported efficient uptake of the YBG vaccine by DCs in vitro that induced significantly higher levels of IFN-γ, IL-4, and IL-17 in $CD4^+$ T cells; in vivo vaccination resulted in significantly higher IgG titers compared to the alum/OVA formulation, a result attributed to improved antigen delivery to DCs via Dectin-1-mediated uptake that results in enhanced antigen presentation to T cells in vivo.[78] Other studies have investigated the combination of traditional adjuvants with YBG to improve delivery efficiency and/or immune response. For example, a combination of YBG and the AS04 adjuvant designed for *T. gondii* vaccination exhibited enhanced lymph node accumulation in mice as well as higher IgG titers and pro-inflammatory cytokines when both YBG and AS04 were present,[77] suggesting that a combination of adjuvants acting via different mechanisms (Dectin-1 and TLR4 activation by YBG and AS04 respectively)[87] may provide augmented immunological responses to vaccines.

In addition to antigen encapsulation, chemical conjugation methods have been utilized to immobilize vaccine components to the surface of glucan microparticles to enhance the presentation of these molecules to immune cells. The abundance of hydroxyl groups on YBG allows for simple conjugation with proteins and peptides via carbodiimide chemistry, as has been demonstrated with YBG-OVA conjugates that can promote DC maturation and T cell activation in vitro.[80] Enzyme-cleavable linkers can also be incorporated into YBG/antigen conjugates, allowing for antigen release in the lysosomes of DCs for more effective cross-presentation to T cells.[79] Additional targeting moieties can also be immobilized on the YBG surface to enhance specific cell targeting and vaccination. For instance, Baert et al. used carbodiimide chemistry to conjugate a monoclonal antibody targeting aminopeptidase N (APN) on YBG to target intestinal epithelial cells for oral vaccination.[81a] In vitro immunomodulation assays showed that while both unmodified YBG and anti-APN YBG could effectively increase TNF-α production in DCs (thus confirming YBG's inherent immunostimulatory effect), anti-APN YBG also yielded significant increases in IL-1β and IL12p40 as well as increased CD40 and CD80 expression indicative of DC activation. Anti-APN YBG also accumulated more effectively in intestinal epithelial cells compared to unmodified YBG in an intestinal explant model, confirming that anti-APN conjugation confers specific intestinal cell targeting to YBG. Consistent with these results, piglets immunized with anti-APN YBG loaded with the FedF antigen showed increased Ig levels compared to FedF alone, suggesting that YBG can provide both targeted delivery and payload protection from the harsh environment of the gastrointestinal tract.

Recent clinical trials have also demonstrated the ability of yeast-derived beta-glucans to increase antibody titers without inducing significant toxicity when combined with vaccines for influenza,[88] COVID-19,[88] and high-risk neuroblastoma.[11] However, these trials administered YBG as a separate oral supplement from the vaccine, making additional studies required to determine the potential benefit of YBG-vaccine composites in a clinical setting.

3.2.3. Targeted Drug and/or Nanoparticle Delivery Vehicles

The hollow core and porous shell structure of YBG allow for the loading of both small molecule and macromolecular payloads while the bioactivity of YBG offers the potential to not only target and deliver drugs to specific cells but also modulate their phenotype. For example, DOX-loaded YBG microparticles can both arrest breast cancer cell growth and stimulate TNF-α and IL-2 secretion from peripheral blood mononuclear cells (PBMC),[57a] resulting in a dual-action chemo- and immunotherapeutic. In vivo, DOX-loaded yeast cells can effectively concentrate in murine tumors compared to free DOX, specifically by accumulating in tumor MΦ due to a combination of particle size and Dectin-1 targeting.[84] It is also worth noting that drug-loaded YBG, even at high loadings, can still be phagocytosed by MΦ to the same extent as unloaded YBG, suggesting that Dectin-1 interactions are not significantly hindered by drug encapsulation.[50] Other studies have shown that YBG can be used as a delivery vehicle for anti-inflammatory applications despite YBG typically exhibiting pro-inflammatory properties. For instance, Sun et al. prepared YBG particles containing the anti-inflammatory drug methotrexate through a dissolution/precipitation method, resulting in a depot of methotrexate precipitates within the YBG core.[57c] The drug-loaded composites were selectively taken up by MΦ in a Dectin-1-dependent manner, thereby minimizing any methotrexate-induced toxicity to intestinal epithelial cells. In vivo, administration resulted in attenuated inflammatory markers in mice with ulcerative colitis to a greater degree than observed with either YBG or methotrexate alone.[57c] Šalamúnová et al. also observed enhanced activity when anti-inflammatory compounds were spray dried with YBG, with treated THP-1-derived MΦ displaying significant reductions in NF-κB activity that is responsible for the transcription of several pro-inflammatory cytokines.[51] Interestingly, in both of these works, YBG treatment alone caused a reduction in pro-inflammatory markers; explanations for this finding were not provided despite these results being in contrast with other findings around YBG. It is possible that differences in YBG purity/particle properties

and/or differences in cell lines/animal models could explain this discrepancy, further highlighting the importance of mechanistic research as well as the need for consistent YBG processing for appropriate comparison of results across the literature.

Several groups have explored the use of NP-loaded YBG microparticles for cell targeting and/or immunomodulation. Soto and Ostroff demonstrated the ability to self-assemble DNA polyelectrolyte complexes within the hollow core of YBG, resulting in improved transfection of Dectin-1-expressing cells compared to unencapsulated polyelectrolyte NPs.[81b] In vivo, YBG can simultaneously act as a MΦ targeting agent while also protecting sensitive payloads from degradation in the gastrointestinal tract given that YBG structural integrity and targeting ability have been shown to be unaffected by simulated gastric fluid.[58a] Other methods including surface binding of anionic mesoporous silica NPs (MSNs) to surface-functionalized cationic YBG,[59a] encapsulation of cationic NPs into the anionic YBG cavity,[59c,d] or encapsulation of peptide-loaded PLGA NPs[59g] have been employed to deliver various therapeutics directly to MΦ or MΦ-populated tissues. Some of these studies further confirmed that MΦ uptake of these YBG-nanoparticle composites remains Dectin-1 mediated, with differential uptake observed with or without the presence of the Dectin-1 antagonist laminarin.[59c,d,g] In some cases, not only the MΦ targeting properties of NP-loaded YBG but also the MΦ modulating properties of YBG are simultaneously leveraged. When YBG encapsulating berberine and epigallocatechin gallate for ulcerative colitis treatment was incubated with anti-inflammatory M2 MΦ, neither YBG alone nor the NP-loaded YBG had a significant effect on the ratio of M2/M1 MΦ; however, when the drug-loaded YBG was incubated with pro-inflammatory M1 MΦ, there was a significant increase in the M2/M1 ratio compared to the LPS control consistent with the enhanced targeting and subsequent NP uptake conferred by YBG.[83] However, this increase was similar to that seen using the NP alone without the YBG component, suggesting that MΦ modulation, in this case, was induced primarily by the immunomodulatory NP and not YBG. Indeed, most of the nano-in-micro YBG formulations in the literature have focused on YBG's targeting and uptake properties, with few studies exploring its immunomodulatory properties despite the obvious benefits of such properties in many proposed applications like cancer and inflammatory diseases. As such, an improved understanding of YBG's immunomodulatory effects may help identify synergistic or confounding effects when combined with the therapeutic NPs as well as how encapsulating versus surface binding the NPs to YBG affects the immunomodulatory response observed.

4. Beta-Glucan Nanoparticles

While yeast-derived microparticles have clear advantages in terms of their ease of production (given that the particle shell is typically pre-fabricated by the yeast cell itself and only needs to be preserved in the drying process to make the microparticles), the relatively large size and rigid structure of YBG limits its use to non-systemic administration methods like oral and pulmonary delivery; indeed, systemic administration of microparticulate BG has been shown to induce undesirable inflammation, granuloma formation, and microembolization.[89] Developing β-1,3 glucan-derived formulations that can be administered systemically but preserve the desired immunomodulatory properties of BG thus has the potential to expand beta-glucans utility as a multi-functional therapeutic by improving its delivery to difficult-to-reach regions like solid tumors and other diseased tissues. On this basis, considerable research effort has been invested in developing nano-scale beta-glucan materials to better target these disease sites. NPs pose several other advantages over microparticles such as 1) a higher surface area to volume ratio,[37] resulting in a higher number of sterically accessible β-1,3 linkages for interactions with immune cells; 2) sizes compatible with cell entry via mechanisms other than phagocytosis (e.g., various endocytosis pathways)[37,90] that may allow for the targeting of an accumulation of the beta-glucans in non-phagocytic cells; and 3) the potential for circulation to enable systemic targeting of the therapeutic to a specific disease site. In this section, we will summarize the current progress on beta-glucan NP formulations and their application as delivery vehicles and immunomodulators.

4.1. Beta-Glucan Nanoparticle Fabrication

4.1.1. Helix Interactions

As discussed in Section 2, many sources of BG adopt single or triple helical structures in aqueous solutions that are primarily attributed to strong intra- and inter-molecular hydrogen bonding between polymer strands.[22] Studies of various helical polysaccharides have shown that these structures can be reversibly broken in response to hydrogen bond disruptors including heat, solvent exchange, and alkalinity,[22] leading to the development of nanoscale BG therapeutics by incorporating molecules into the helix during the renaturation process. A schematic of the denaturation/renaturation process, along with other common BG NP fabrication techniques, is illustrated in **Figure 4**; a summary of these techniques is provided in **Table 2**. In particular, several studies have demonstrated the incorporation of DOX into BG helices for cancer applications. The successful formation of these NPs typically requires either molecular weight reduction[91] or hydrophobic modification,[92] resulting in particle sizes around 200 nm but as low as 70 nm. Due to the binary nature of these systems, DOX often comprises a significant weight fraction of the system, with loadings as high as 41 wt.% reported.[91a] Furthermore, the primary amine on DOX allows for pH-responsive release by both enhancing DOX solubility and disrupting the chiral and hydrogen bonding interactions with the BG triple helix, with heightened burst release at lower pH values sometimes achievable in poorly vascularized and rapidly growing tumours (pH 5–6.5) compared to pH 7.4 to improve tumor targeting.[91,92b]

In addition to small molecules like DOX, helix denaturation/renaturation can also be used to incorporate macromolecules into the helical structure using similar formulation conditions. Nucleic acids of varying structures including single stranded DNA (ssDNA),[110] CpG oligonucleotides (CpG),[107a] small interfering RNA (siRNA),[108] and aptamers[106] have been successfully assembled with triple helical BGs including Zymosan, lentinan (a mushroom-derived β-1,3 glucan),[106] and schizophyllan (SPG, from *Schizophyllum commune*).[26] However, in many cases, direct complexation does not proceed efficiently due to insufficient chain lengths, conformations, or hydrogen

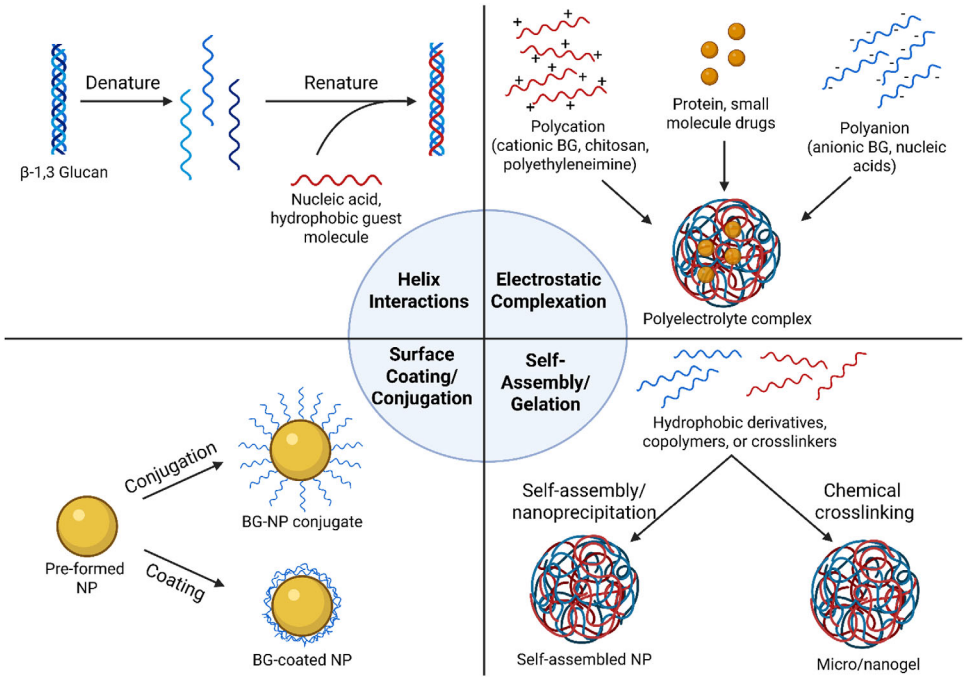

Figure 4. Schematic representation of the major fabrication methods for beta-glucan NPs including both covalent (crosslinking, surface conjugation) and noncovalent (hydrophobic, electrostatic, hydrogen bonding, and helix interactions) assembly methods to fabricate NPs based on both BG and BG derivatives. Created with Biorender.com.

bonding capacity.[106,111] To address this, nucleic acids are often modified with poly(deoxyadenylic acid) (poly(dA)) to improve the hydrogen bonding interactions between the nucleic acid and the BG chains. Minari et al. demonstrated that SPG could be denatured in NaOH and renatured in the presence of poly(dA)-modified CpG to form composite glucan/CpG triple helices with complexation efficiencies between 78%–100%.[107a] The same group showed that poly(dA) modification can also be used to directly complex OVA with SPG.[107b] Similar complexes were prepared by Duan et al. from poly(dA)-modified aptamers and lentinan,[106] although the size and complexation efficiency were not fully quantified.

Some nucleic acids, depending on their length and hydrogen bonding ability, can be complexed with BGs without additional modification. For example, ssDNA can be complexed with trifluoroacetic acid (TFA)-hydrolyzed Zymosan via denaturation/renaturation with DMSO and water, respectively. Depending on the extent of hydrolysis, NPs of 300, 500, or 800 nm can be obtained with DNA complexation yields of up to 50%[110] attributed to strong hydrogen bonding interactions. Similarly, TFA-treated SPG can complex siRNA to fabricate NPs with a diameter of ≈300 nm and DNA loadings of ≈67%.[108] One other interesting study assessed the complexation mechanisms of a cationic curdlan with various guest molecules including polycytidylic acid (poly(C)) as well as hydrophobic molecules like permethyldecasilane (PMDS) and single-walled carbon nanotubes (SWNTs).[109] The cationic curdlan adopted a single helix conformation that could either form helical composites with poly(C) or incorporate guest molecules inside the helix through the complexation process shown in **Figure 5**, a response attributed to a combination of hydrogen bonding, pi-pi stacking, and electrostatic interactions without the need for a sequential denaturation/renaturation processes.[109] However, the loading and release of these compounds were not quantified, such that further investigation is required to determine the suitability of these complexes as nanoscale delivery vehicles. Overall, the use of supramolecular assembly for fabricating BG nanoparticles offers clear benefits of simple formulation and minimal modification to the physicochemical properties of the glucan but can limit the types of assemblies formed according to the physicochemical properties (and inherent variability) of the BG starting materials.

4.1.2. Electrostatic Complexation of Charged Glucan Derivatives

As an alternative to supramolecular assembly, BGs can be chemically functionalized with a wide range of ionic moieties including carboxyl, amino, sulfate, and quaternary ammonium groups to enable the formation of polyelectrolyte complexes (PECs) between two oppositely charged BGs or a charged BG and a charged drug. Such electrostatic complexation occurs spontaneously in water, driven by an increase in system entropy due to the displacement of counterions surrounding the polymer's charged groups.[112] Major advantages of PECs include their ease of fabrication (provided the initial materials are ionic), their potential to eliminate the use of organic solvents, and their potential to load diverse therapeutic targets, as summarized in the following sections. However, the need to introduce a charge on the inherently neutral BG represents a drawback of implementing this strategy to form BG-based nanoparticles. Furthermore, chemical functionalization of the BG can alter its immunomodulatory effects (both positively and negatively),[89b,113] with relatively few

Table 2. Properties of BG NPs prepared by helix interactions and/or electrostatic complexation.

BG Material	Other NP Components	Fabrication Method	NP size	Drug Loading	Long-Term Stability	Release Profile	Refs.
BG (carboxymethylated)	Protamine sulfate, CpG	Electrostatic complexation	≈300 nm	EE% ≈97%	Not specified	50% release sustained over 72 h	[93]
BG (sulfated) from *H. erinaceus*	Chitosan, resveratrol	Electrostatic complexation	172–191 nm	EE% = 92% LC% = 5%	Stable in water for 18 days; highly sensitive to ionic strength	38% release over 4 h	[94]
Curdlan (carboxymethylated)	*N*-trimethyl chitosan, bovine serum albumin	Electrostatic complexation	≈153–616 nm	EE% up to 89.8%	Stable at 4 °C for up to 12 weeks	Not specified	[95]
Curdlan (sulfated)	Chitosan, rifampicin, D-pinitol	Electrostatic complexation	≈300–500 nm	LC% = 13.2% (D-pinitol) LC% = 24.5% (rifampicin)	Not specified	Initial burst, sustained over 3 days	[96]
Curdlan (sulfated)	Chitosan, zidovudine	Electrostatic complexation	≈100–200 nm	EE% up to 85% LC% up to 11%	Not specified	pH-responsive; initial burst, plateau after 3 days	[97]
Curdlan (sulfated)	Quaternary ammonium-modified chitosan, SARS-CoV-2 spike receptor binding domain	Electrostatic complexation	≈126 nm	EE% = 59%	Not specified	Not specified	[98]
YBG (3-boronobenzoic acid-modified)	Chitosan, phycocyanin/lutein NPs	Electrostatic complexation	≈53–83 nm	EE% up to 95.9% LC% up to 1.2%	Not specified	Sustained release in simulated GI tract fluids over 7 h	[99]
YBG (aminated)	CpG and ovalbumin	Electrostatic complexation	≈184–214 nm	EE% = 82.2% (ovalbumin) EE% = 85.7% (CpG)	Stable for 5 weeks at 4 °C, 6 days at 37 °C	Initial burst, then sustained over 5 days	[100]
YBG (aminated)	pDNA	Electrostatic complexation	118–203 nm	Not specified	Minimal pDNA degradation over 12 h	Not specified	[101]
YBG (carboxymethylated)	Chitosan, ovalbumin	Electrostatic complexation	≈160–170 nm	EE% = 46% LC% = 3.6%	Stable at 4 °C for 2 months; properties preserved after lyophilization	Not specified	[102]
YBG (oxidized)	Aminated glycogen, CpG	Electrostatic complexation	≈180 nm	EE% ≈99% LC% = 7.3%	Not specified	Enzyme-responsive burst release	[103]
YBG, curdlan (aminated)	siRNA, dsDNA, pDNA	Electrostatic complexation	≈93–203 nm	Not specified	Not specified	Not specified	[101,104]
Zymosan (sulfated)	Polyethylene glycol-*b*-polyethyleneimine doxorubicin	Electrostatic complexation	≈31–127 nm	EE% = 64%	Not specified	pH responsive; initial burst, then sustained over 10 days	[105]
Curdlan (hydrolyzed)	Doxorubicin/ curdlan complexes coated in red blood cell membranes	Helix interactions	≈90–110 nm	Not specified	Not specified	pH responsive; burst at pH 5.4	[91b]
Lentinan	Polydeoxyadenylic acid-modified aptamers	Helix interactions	Not specified	Not specified	Not specified	Not specified	[106]
Schizophyllan	Ovalbumin and/or polydeoxyadenylic acid-modified CpG	Helix interactions	Not specified	Up to 8 CpG molecules/ complex; ≈100% ovalbumin complexation	Not specified	Not specified	[107]
Schizophyllan (hydrolyzed)	siRNA	Helix interactions	≈300–400 nm	EE% = 67%	Not specified	Not specified	[108]

(*Continued*)

Table 2. (Continued)

BG Material	Other NP Components	Fabrication Method	NP size	Drug Loading	Long-Term Stability	Release Profile	Refs.
Schizophyllan, curdlan (aminated)	Polycytidylic acid, permethyldecasilane, single-walled carbon nanotubes	Helix interactions	Height: 1–2.5 nm Length: 150–200 nm	0.8 PMDS molecules per repeat unit	Complexes with polycytidylic acid or carbon nanotubes stable for 1 month (data not shown)	Not specified	[109]
YBG (butyrylated or depolymerized)	Doxorubicin	Helix interactions	≈70–200 nm (depolymerized) ≈90–300 nm (butyrylated)	EE% up to 38% LC% up to 39%	Stable for 2 months (data not shown)	pH responsive; burst at pH 5.0	[92b]
Zymosan (hydrolyzed)	Doxorubicin	Helix interactions	≈190–290 nm	EE% = 80% LC% = 41%	Not specified	Controlled, pH responsive	[91a]
Zymosan (hydrolyzed)	ssDNA	Helix interactions	≈300–900 nm	EE% = 50%	Not specified	Not specified	[110]
YBG (formate, acetate, hexanoate modified)	N/A	Helix interactions, hydrophobic self-assembly	132–487 nm	N/A	Not specified	N/A	[92a]

papers explicitly probing how modifying the BG chemistry alters immune cell interactions and activity.[114] As such, BG functionalization must be conducted by balancing the potential for fabricating more stable and chemically diverse nanoparticles with the potential for decreased immunomodulatory potential and immune cell receptor affinity.

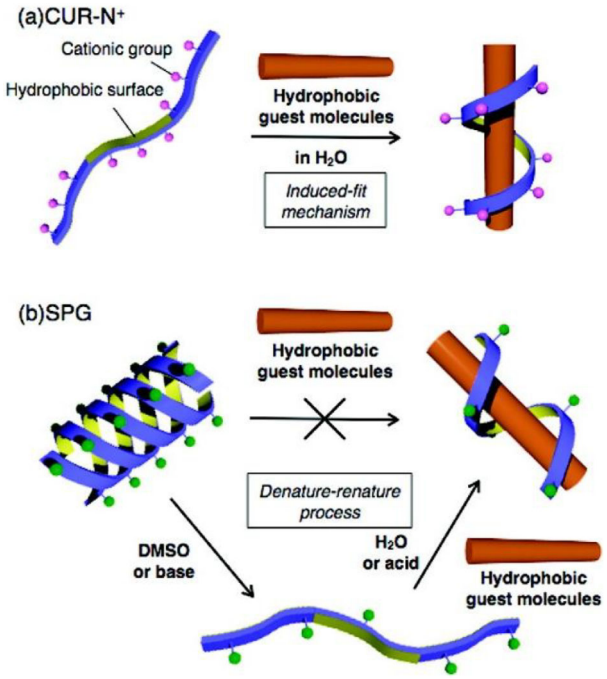

Figure 5. Differences in helical interactions between cationic curdlan ($CUR\text{-}N^+$) and schizophyllan (SPG) with hydrophobic guest molecules by which the cationic curdlan forms complexes without an intermediate denature-renature step. Reproduced with permission.[109] Copyright 2007, American Chemical Society.

Nucleic Acid Complexation: The synthesis of cationic BG derivatives enables spontaneous complexation with nucleic acids due to (1) the improved aqueous solubility of charged BG derivatives; and (2) the electrostatic complexation between the cationic group on BG and the anionic phosphate groups present on nucleic acids. Various cationic moieties have been introduced along the BG backbone to enable nucleic acid loading. For example, primary amino groups can be introduced to the C6 position of curdlan via azidation followed by sodium borohydride reduction,[104a] with the resulting polymer used to form PECs with siRNA of sizes 93–183 nm with significantly less toxicity compared to other gene delivery vehicles like polyethyleneimine (PEI).[115] The same group further demonstrated that azido-functionalized curdlans could be modified using "click" chemistry techniques, as illustrated in **Figure 6**.[104b] Through simple mixing with dsDNA, nanocomplexes of ≈200 nm diameter with positive zeta potentials were formed, suggesting an excess of curdlan-lysine on the surface;[104b] interestingly, curdlan-lysine alone formed ~300 nm NPs in PBS, suggesting the potential for self-assembly of the amphiphilic conjugate and the role of the dsDNA to condense the particles due to strong lysine/dsDNA interactions.

In addition to curdlan, ethylenediamine-functionalized YBG has been used for nucleic acid complexation, showing the ability to simultaneously complex both CpG-ODN and OVA via dropwise nanoprecipitation into ternary complexes of diameter ≈184 nm and EE% > 80% for both payloads.[100] This ternary complex is particularly interesting as it consists of two distinct immunopotentiators with distinct modulation mechanisms (YBG and CpG-ODN) and an antigen payload (OVA), offering the potential for enhanced immune response to the antigen. Other YBG-based polyelectrolyte complexes have been developed by first crosslinking oxidized YBG with aminated glycogen via a Schiff-base reaction followed by electrostatic complexation of the excess amino groups with CpG-ODN to yield a PEC (diameter ≈180 nm and EE%'s up to 99%) with YBG moieties on the surface for immune recognition that can enable stimulus-responsive

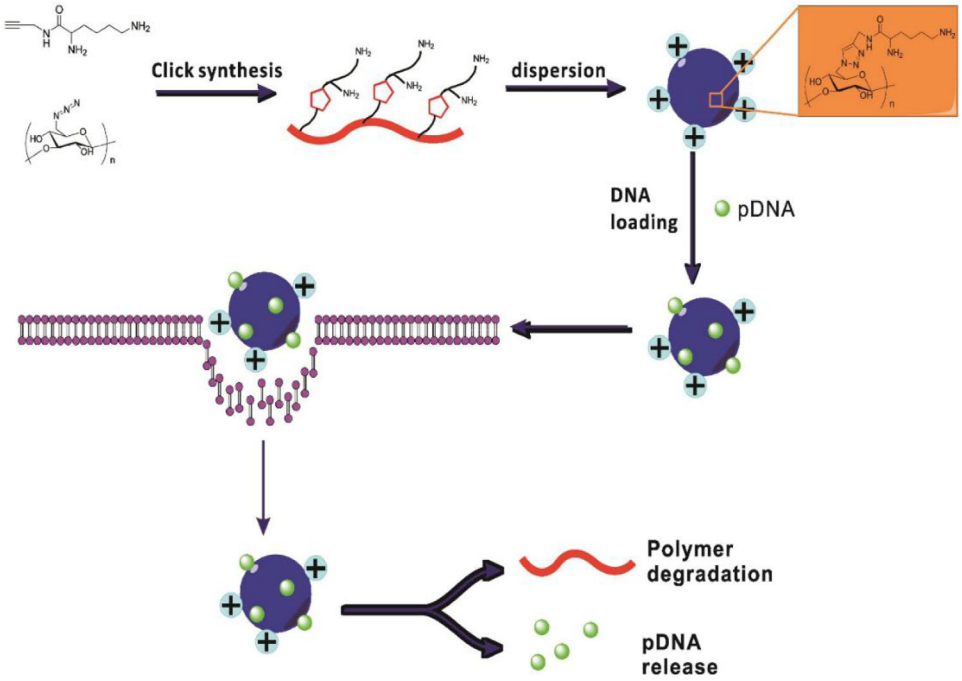

Figure 6. Schematic illustrating the amination of azido-curdlan via click chemistry, assembly into pDNA-loaded NPs, and subsequent cell internalization and intracellular drug release of the resulting NPs. Reproduced with permission.[104b] Copyright 2017, Elsevier.

release of CpG-ODN in the presence of glycogen-degrading α-glucosidase.[103]

Small Molecule Loading/Complexation: Several ionic as well as neutral small molecule drugs have also been incorporated into BG-containing PECs, allowing for the targeted delivery of these molecules to enhance efficacy and minimize toxic side effects. While direct complexation between oppositely charged polymers and drug molecules is possible, most drug-loaded PECs consist of two oppositely charged polymers (to promote efficient PEC formation) into which the drug is encapsulated through physical entrapment and/or electrostatic interactions. Derivatives of curdlan and YBG are commonly used β-1,3 glucans for PEC formulation, with complexes between curdlan sulfate (prepared via sulfur trioxide/pyridine complex sulfation) and chitosan particularly used to encapsulate a wide range of drugs including zidovudine, rifampicin, and D-pinitol; zidovudine-loaded PECs have been prepared with diameters ≈186–196 nm[97] while co-loading of rifampicin and D-pinitol yields much larger PECs of diameters ≈500 nm,[96] with both systems yielding high drug loading capacities ranging from 11–24.5 wt.%. Low pH, high sulfate/amine ratios, and low polymer concentrations were reported to enable the production of optimally small and stable PECs using the curdlan sulfate/chitosan system.[96] This PEC system also demonstrated good cytocompatibility in RAW 264.7 MΦ, L929 fibroblasts, and A549 epithelial cells, with significantly enhanced uptake in the MΦ likely due to a combination of the relatively large size of the PECs and the affinity of the PECs for Dectin-1 receptors expressed on the MΦ.[96]

Other groups have explored the use of YBG derivatives as the bioactive component in PEC formulations. Sulfated Zymosan has been complexed with PEGylated PEI in the presence of DOX to yield PECs with dual chemo- and immune-therapeutic properties.[105] Using a dropwise nanoprecipitation technique, PECs with sizes ranging from 31–127 nm were formed with polydispersity indices as low as 0.192. DOX was most efficiently loaded (EE% = 74%) at higher Zymosan concentrations, suggesting that electrostatic interactions between DOX hydrochloride and Zymosan sulfate play a key role in drug encapsulation, and release was accelerated in acidic conditions, beneficial for cancer applications in which the acidic tumor microenvironment may promote accelerated release at the disease site compared to healthy tissues.[116] Another YBG-derived PEC was recently reported by Liu et al. using the layer-by-layer (LbL) assembly method,[99] leveraging the sequential surface coating of a particle with polymers of alternating charge to both tune the surface chemistry as well as load multiple therapeutics within specific layers of the LbL assembly. Specifically, lutein/phycocyanin NPs were coated with positively charged chitosan followed by a final coating with negatively charged 3-boronobenzoic acid-modified YBG, yielding NPs with sizes ≈82 nm, high EE% and LC% (96% and 12%, respectively), improved protection of lutein from heat/UV irradiation, and prolonged release times in simulated saliva, gastric, and intestinal fluids over 7 hours.[99]

An important property to consider during PEC design and characterization is PEC stability, particularly as a function of ionic strength. Since PECs form primarily through electrostatic interactions, they are often highly sensitive to high salt concentrations that can destabilize the particles through charge screening effects.[117] However, PECs are often prepared in pure water or dilute salt conditions, and their subsequent stability in high ionic strength media is often not characterized. A noteworthy example of the importance of testing PEC stability in various conditions was demonstrated by Jin et al., who prepared the CpG/OVA/aminated glucan PECs and showed a broaden-

ing of the particle size distribution over 6 days at 37 °C in PBS but retained colloidal stability with no signs of significant aggregation.[100] In contrast, while Cordeiro et al. reported OVA-loaded PECs using carboxymethylated YBG and chitosan that maintained similar sizes and PDIs after 28 days at 40 °C,[102] all tests were performed in pure water and salt-induced charge screening effects were not considered. Similarly, while a library of 20 PECs prepared from carboxymethyl curdlan with chitosan chloride or *N*-trimethyl chitosan in water resulted in 19 formulations that retained colloidal stability in water over a 12-week test period, stable PECs could not be formed in other media such as 0.9% saline and PBS.[95] Incorporating physiologically relevant stability studies into the PEC optimization process is thus essential to better identify formulations that will perform effectively and more predictably in the more complex in vitro and in vivo environments.

4.1.3. Beta-Glucan Surface Coatings & Conjugates

An alternative method to leverage the targeting/immunomodulation benefits of BG in nanoparticle formulations is to modify the surface of pre-existing NPs with BG for targeting, compatibility, and/or immunomodulation purposes, allowing the use of a wider variety of NPs with specific drug loading/release properties or sizes while providing control over particle surface chemistry. A summary of NP formulations leveraging BG-based surface coatings and surface conjugates is provided in **Table 3**.

Beta-Glucan Surface Coatings: Due to the abundance of hydroxyl groups along the BG backbone, NPs of various surface chemistries can be modified by adsorbing BG onto the surface through hydrogen bonding interactions. This technique has been applied to a variety of inorganic NPs to improve both their targeting ability as well as their aqueous stability. For example, superparamagnetic iron oxide NPs (SPIONs) have been coated with BG to improve their MΦ-targeting properties for applications in both cancer diagnosis and treatment,[32b,118] with BG coatings yielding highly stable NPs of size ≈30–50 nm with a clear core/shell morphology as observed by TEM.[32b] Alternately, inorganic NPs can be formed in the presence of BG, a process in which BG acts as a stabilizing agent during the particle fabrication process. This process has been demonstrated via the radiation-promoted synthesis of selenium NPs as well as the synthesis of peptide-conjugated gold NPs;[119] in both cases, sub-100 nm NPs can be produced with a water-swollen BG shell that promotes extended colloidal stability, with BG-coated selenium NPs remaining colloidally stable over 60 days due to the steric stabilization provided by the long, hydrophilic BG chains.

BGs have also been used as surface coatings for polymer-based NP formulations. Dube et al. prepared rifampicin-loaded NPs of size ≈280 nm from PLGA and chitosan oligosaccharide lactate via an emulsion-solvent evaporation method followed by incubation with BG derived from *Euglena gracilis*.[120] Despite the short BG incubation time (10 minutes), BG coating was indirectly confirmed in vitro by the enhanced uptake of the NPs by human alveolar-like MΦ compared to the uncoated PLGA-chitosan NPs. BG coatings can also be applied to pre-formed PECs, combining the benefits of high throughput NP formulation via electrostatic complexation with simple surface adsorption of BG. This strategy has been demonstrated with PECs prepared from plasmid DNA complexed with a combination of poly(*β*-amino ester)s and poly[2-(dimethylamino)ethylmethacrylate] (PDMAEMA) that were subsequently incubated with water-soluble YBG prepared using a high temperature/pressure solubilization method,[121] resulting in particle sizes of ∼180 nm that remained stable for at least 48 h both at room temperature and 4 °C. Another PEC formulation consisting of chitosan and tripolyphosphate (TPP) loaded with paclitaxel was coated with BG from *E. gracilis* via a hypothesized combination of non-covalent and ionic interactions for applications in glioblastoma therapy,[122] with 1% BG yielding NPs with increased size and PDI (161 nm and 0.243, respectively) compared to the uncoated NPs but good colloidal stability over 45 days in water at 2–8 °C (although stability under physiologically-relevant temperature and ionic strength was not considered). TEM imaging clearly showed the formation of a ≈20 nm surface coating surrounding the chitosan/TPP core that provided an additional diffusion barrier during paclitaxel release, resulting in a less pronounced burst and more consistent release over 96 hours compared to uncoated PECs.

Beta-Glucan Surface Conjugates: While physical adsorption of pre-existing NPs with beta-glucans enables the incorporation of BG into nanoformulations in a simple, time-efficient manner, BG's abundant hydroxyl groups also allow for conjugation with a wide range of functional groups to not only expand the range of materials available for BG functionalization but also introduce improved control over surface coverage density and stability over time. A schematic outlining common BG/NP conjugation methods is shown in **Figure 7**.

The most common BG conjugation chemistry is carbodiimide chemistry, which enables the formation of ester or amide linkages in water under ambient conditions depending on the functionality of BG and the corresponding NP. An example of this technique was illustrated by Cheng et al., in which YBG was conjugated to graphene oxide (GO) nanosheets via activation of the carboxyl groups of GO with 1-ethyl-3-[3-dimethylaminopropyl]carbodiimide (EDC) followed by esterification with the hydroxyl groups on YBG.[126] The grafting efficiency of YBG was determined to be 21.5%, resulting in a BG surface coverage that could reduce protein adsorption in serum, promote colloidal stability for >48 h in PBS, and enhance the cytocompatibility of the GO platform while still providing room for loading of CpG oligodeoxynucleotides via hydrogen bonding and pi-pi stacking with GO to balance colloidal stability with therapeutic loading (**Figure 8**).[126] Other carbon allotropes such as fullerenes have been selected for BG conjugation due to their lower toxicity and applications in reactive oxygen species (ROS) scavenging, typically by functionalizing the fullerenes with amino or carboxyl groups followed by an amidation reaction to conjugate aminated or carboxylated curdlan on the fullerene surface.[125] NPs with sizes ranging from 78 to 163 nm can be obtained using these methods through a combination of electrostatic interactions, water molecule polarization, and intermolecular hydrogen bonding,[125b] with the presence of curdlan improving MΦ recognition in vitro and suppressing NP precipitation in FBS and DMEM media (although stability as a function of time was not discussed).

Table 3. Properties of BG NPs prepared via surface coating/conjugation and self-assembly and/or crosslinking.

BG material	Other NP Components	NP fabrication method	NP size	Drug loading	Long-term stability	Release profile	Refs.
BG (carboxylated)	Ovalbumin, mesoporous silica NPs	Surface conjugation	≈111–253 nm	EE% ≈58% LC% ≈52%	Not specified	Not specified	[123]
Curdlan	Carboxyl-terminated PLGA, rifampicin	Surface conjugation	≈301–487 nm	LC% ≈0.1 wt.%	Not specified	Burst release at 1 h, plateaued over 6 h	[124]
Curdlan (aminated, carboxymethylated)	Fullerene	Surface conjugation	≈78 nm; ≈163 nm	N/A	No precipitation in cell media	N/A	[125]
YBG	Graphene oxide, CpG	Surface conjugation	≈200–220 nm	LC% ≈3%–3.5%	Stable in PBS for 48 h	Not specified	[126]
YBG (hydrolyzed, soluble)	Polystyrene NPs	Surface conjugation	≈48–200 nm	1.4–4.4 µg YBG/mg	Not specified	N/A	[127]
YBG (low MW)	$BaTiO_3$ NPs	Surface conjugation	≈50–60 nm	YBG content ≈7.8–10.7 wt.%	Stable in PBS at RT for 14 days	N/A	[128]
BG (periodate oxidized, source not specified)	Insulin, keratin, β-cyclodextrin	Surface coating	≈258 nm	EE% = 98% LC% = 33%	Not specified	Reduced burst release when coated with BG	[129]
BG from *E. gracilis*	Paclitaxel-loaded chitosan/tripolyphosphate NPs	Surface coating	≈113–336 nm	EE% ≈80%	22% size increase after 45 days at 4 °C	Sustained release over 4 days	[122]
BG from *E. gracilis*	Rifampicin-loaded chitosan/PLGA NPs	Surface coating	≈280 nm	≈24 µg drug per mL of NP suspension	Not specified	Not specified	[120]
Not specified	Superparamagnetic iron oxide NPs	Surface coating	≈52 nm	N/A	Not specified	N/A	[118]
YBG	$CaCO_3$ NPs	Surface coating	≈173 nm	N/A	Stable in media for 24 h	N/A	[130]
YBG	Ferumoxytol	Surface coating	≈30 nm	Not specified	Stable in 10% fetal bovine serum over 24 h	pH responsive release of YBG over 6 days	[32b]
YBG	Gold NPs, MUC4 glycopeptide	Surface coating	≈38–48 nm	≈362 nM peptide in 400 µg mL^{-1} NP solution	Not specified	Not specified	[119b]
YBG	Zn/doxorubicin complexes	Surface coating	≈150 nm	EE% up to 81%; LC% up to 21%	Stable in powder form over 8 weeks	Not specified	[131]
YBG (acid, temperature, pressure treated, soluble)	DNA complex with poly[2-(dimethylamino)ethyl methacrylate] and poly(β-amino ester)s	Surface coating	≈180 nm	Not specified	Stable for 48 h at room temperature	Not specified	[121a]
YBG (low MW)	Selenium NPs	Surface coating	650-110 nm	N/A	44% size increase after 60 days at 25 °C	N/A	[119a]
Curdlan (aminated)	Curdlan NPs, epichlorohydrin crosslinker	Self-assembly + crosslinking	≈523–595 nm	N/A	No significant size change in PBS after 3 days	N/A	[132]
Curdlan gum	Gallic acid, glutaraldehyde	Self-assembly + crosslinking	≈80 nm	EE% = 88% LC% = 8%	Payload stability for 80 h from pH 3.4–9.2	≈80% release after 48 h	[133]
YBG	Methoxy-PEG, 3, 3′-dithiodipropionic acid crosslinker, methotrexate	Self-assembly + crosslinking	≈300–348 nm	LC% = 23.7%	Not specified	pH- & glutathione-responsive burst release	[134]
BG (carboxymethylated) from *P. tuber-regium*	Superparamagnetic iron oxide NPs	Self-assembly	≈193 nm	Not specified	Stable in 10% fetal bovine serum for 24 h	Enhanced iron release compared to blank NPs over 6 h	[135]

(*Continued*)

Table 3. (Continued)

BG material	Other NP Components	NP fabrication method	NP size	Drug loading	Long-term stability	Release profile	Refs.
BG (carboxy-methylated, phosphorylated, source not specified)	Ovalbumin, aluminum hydroxide	Self-assembly	66–119 nm	EE% = 89%–91%	Stable in water for 72 h	Not specified	[136]
BG from *Inonotus obliquus*	Tripolyphosphate	Self-assembly	≈68 nm	N/A	Not specified	N/A	[137]
Curdlan	Pluronic F-127, rifampicin- or levofloxacin-loaded cyclodextrin	Self-assembly	≈226–523 nm	LC% up to 6%	Not specified	Initial burst; 70%–80% release after 72 h	[138]
Curdlan	Poly(γ-glutamic acid)	Self-assembly	≈200–300 nm	N/A	Stable in water for 9 days	N/A	[139]
Curdlan	Tween 80, curcumin	Self-assembly	111–398 nm	EE% = ≈100%	130 nm NPs stable in water at RT for 42 days	Not specified	[140]
Laminarin	Poly(ethylene glycol)-poly(lactic acid) polymersomes	Self-assembly	≈100–400 nm	N/A	Stable for 48 h in media	N/A	[141]
YBG (acetylated)	Polydopamine	Self-assembly	≈297 nm	N/A	Stable in media/serum for 3 days	N/A	[142]
YBG (low MW)	Doxorubicin or temozolomide prodrug	Self-assembly	≈74 nm	EE% = 90% LC% = 25%	Stable in water at 4 °C for 2 months	Enhanced release from M1 MΦ compared to M0 MΦ	[143]
YBG (oxidized)	Cefotaxime prodrug	Self-assembly	≈200 nm	EE% up to 82%; LC% up to 24%	Stable in water for 30 days at 4 °C	ROS-dependent release over 48 h	[144]
Zymosan (low MW)	mRNA, lipid NPs	Self-assembly	≈104 nm	EE% = 85%	Stable in PBS for 14 days at 4 °C	Not specified	[145]
Zymosan (oxidized)	mRNA, lipid nanoparticles	Self-assembly	83–108 nm	EE% = 79%–98%	Stable in PBS for 14 days at 4 °C	Not specified	[145]
Schizophyllan (methacrylated)	Methacrylated hyaluronic acid (HA), ovalbumin	Direct crosslinking	≈100–300 nm	3 ovalbumin molecules per HA chain	Stable in PBS at 37 °C for 10 days	Not specified	[146]

β-1,3 glucan has also been used to covalently modify other classes of inorganic NPs as well as polymeric NPs.[123,124,127a,128] For example, Lima et al. oxidized soluble YBG with sodium periodate followed by a reaction with carbohydrazide and subsequent sodium cyanoborohydride reduction to yield a stable terminal hydrazide group[127a]; conjugation to COOH-terminated polystyrene was then performed via EDC chemistry, resulting in NPs of sizes 199, 92, and 48 nm with glucan contents up to 4.5 µg per mg of NPs. YBG can also be functionalized with carboxyl groups for surface functionalization of aminated MSNs via similar amidation chemistry, resulting in sizes ranging from 111–253 nm, polydispersity indices < 0.2, and improved in vitro cytocompatibility compared to pure MSNs (although neither the source of YBG nor the carboxylation procedure were clearly disclosed).[123] Finally, a recent study demonstrated the functionalization of $BaTiO_3$ NPs with YBG for applications in targeted colon cancer therapy by partially degrading YBG using hydrogen peroxide[143] and then surface conjugating the resulting aldehyde-functionalized YBG to hydroxylated $BaTiO_3$ NPs via the Mitsunobu reaction to yield an ester linkage, resulting in cubic NPs with size ≈50 nm, glucan contents of 7.8–10.7 wt.%, high colloidal stability in PBS for over 14 days, and rapid Dectin-1-mediated uptake by RAW264.7 cells without inhibiting the piezoelectric and subsequent ROS generating effect of $BaTiO_3$.[128] The stability of each of these grafted coatings offers a particular advantage over physically adsorbed coatings in the context of these multi-functional nanoparticles in which ROS generation or other stimulus-activation properties may influence the stability of an adsorbed coating layer.

4.1.4. Hydrophobic Interaction-Driven Self-Assembly

Hydrophobic interactions, either alone or in combination with electrostatic interactions, hydrogen bonding interactions, or covalent grafts as described above, can be leveraged to drive NP self-assembly in aqueous solution from amphiphilic BG derivatives (see Table 3 for a summary of the reported formulations). An effective example of this technique was reported by Miao et al., in which the hydrophobic drugs DOX or temozolomide (TMZ)

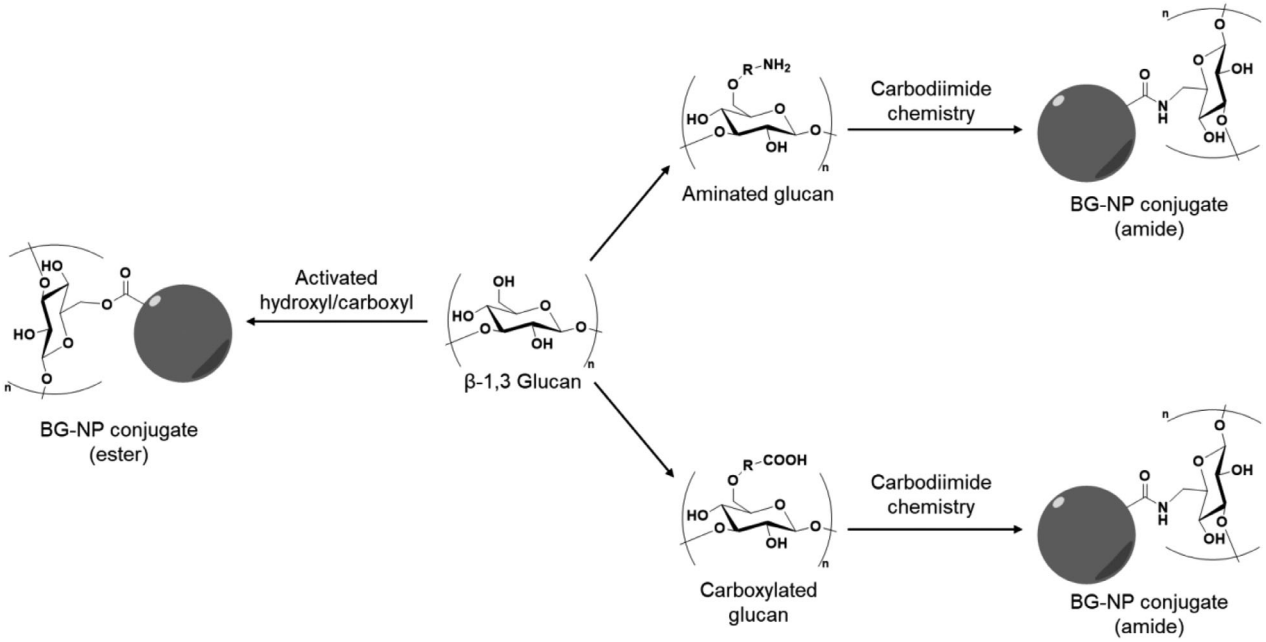

Figure 7. Overview of the common chemical strategies employed to prepare beta-glucan/nanoparticle (BG-NP) conjugates. Carbodiimide chemistry is the most commonly employed method as it is compatible with both carboxylated and aminated glucans, yielding NP conjugates with an amide linkage. Alternatively, the hydroxyl groups on BG can be reacted with carboxylated NPs to yield NPs with an ester linkage.

were conjugated along the backbone of peroxide-degraded YBG to impart both amphiphilicity and drug loading in a simple step (**Figure 9**).[143] The amphiphilic prodrugs could self-assemble in water into NPs with sizes of ≈74 nm and spherical shapes with a "prickly" surface morphology, which the authors attributed to the long, hydrophilic BG chains extending out from the hydrophobic, drug-rich core.[143] Directly conjugating the drugs to the YBG backbone also allowed for high drug loading (12–038 wt.% depending on the feed ratio of drug/polymer), although very high feed concentrations of drug (125:1 to 1000:1 drug/polymer) were required to achieve these high loadings and feed ratios above 500:1 resulted in large aggregates due to the highly hydrophobic nature of these drugs. Thus, hydrophobic interactions must be balanced with other colloidal stabilization techniques (electrostatic, steric stabilization, etc.) to yield small, stable NPs.

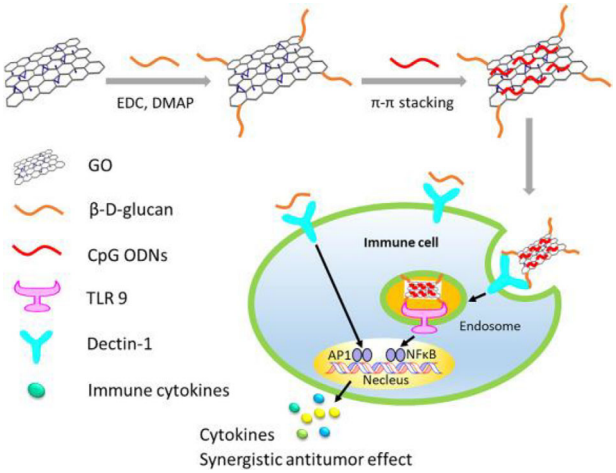

Figure 8. Schematic illustrating the conjugation of BG to GO (via carbodiimide chemistry), loading with CpG, and subsequent uptake by immune cells for effective immunomodulation in cancer therapy. Reproduced with permission.[126] Copyright 2023, Elsevier.

4.1.5. Hydrogen Bond-Driven Self-Assembly

Self-assembly into NPs can also be achieved by utilizing hydrogen bonding as the main driving force. For example, hydrogen bonding interactions between curdlan and poly(γ-glutamic acid) (PGA) enabled the fabrication of NPs of size ≈169 nm that remained colloidally stable for nine days at pH 7.0 by simple mixing in dilute NaOH.[139] Techniques like NMR diffusion-ordered spectroscopy (DOSY) and nuclear Overhauser effect spectroscopy (NOESY) identified hydrogen bonding between curdlan's hydroxyl groups and PGA's amide groups as the main assembly mechanism, a particularly appealing assembly strategy as it avoids the need for any additional polymer modification. However, the stability of these complexes in more complex biological fluids with diverse competitive hydrogen bonding capacities was not assessed and may pose a translational challenge to the practical implementation of this technique.

4.1.6. Surfactant-Driven Self-Assembly

The controlled precipitation of BGs in the presence of surfactants or other co-precipitates can also be leveraged to fabricate BG-based nanoparticles. For example, the precipitation of curdlan in the presence of Pluronic F-127 or Tween 80 resulted in tunable

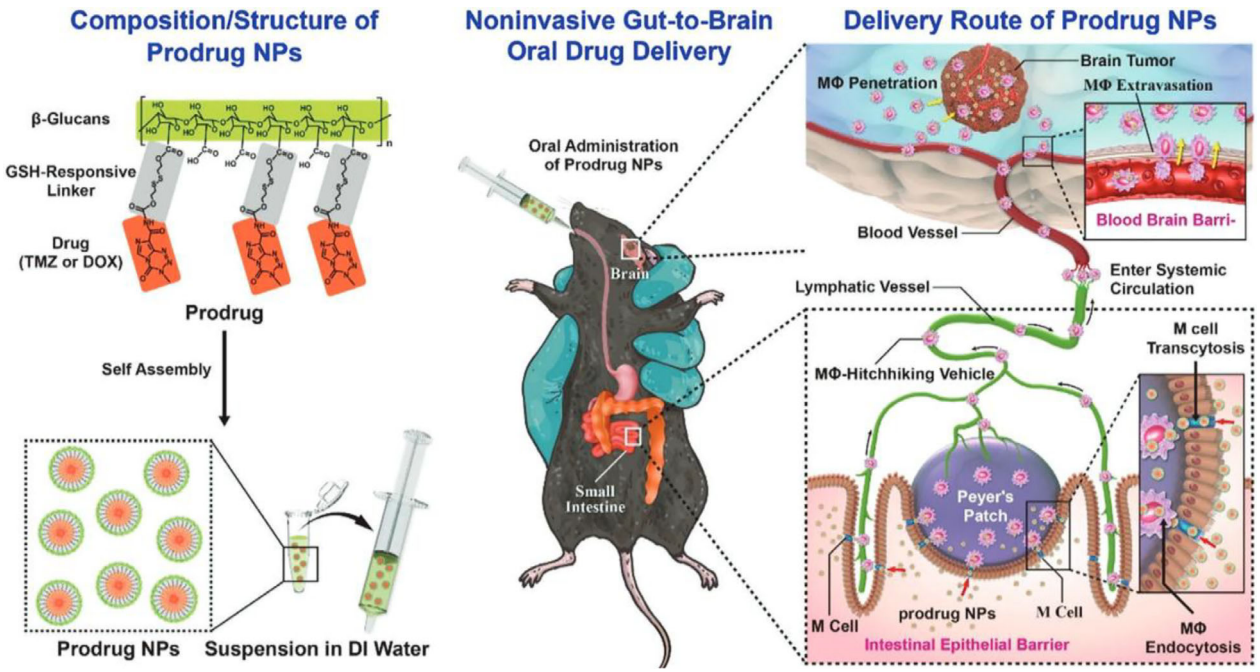

Figure 9. Schematic highlighting the structure, self-assembly, and biodistribution of amphiphilic YBG/DOX or YBG/TMZ prodrug NPs. NPs were fabricated via hydrophobic self-assembly in water and can be taken up by Peyer's patches in the gut following oral delivery, enabling NP transport into systemic circulation through the lymphatic system. Reproduced with permission.[143] Copyright 2021, Wiley.

NP sizes according to the initial glucan concentration, with sizes ranging from 130–355 nm and improved stability as a function of size.[138,140a] Interestingly, not only stability but also cytotoxicity varied with size, as the smaller NPs showed significant toxicity to human PBMCs at concentrations over 100 μg/mL while the larger particles were nontoxic even at concentrations above 600 μg mL^{-1}. As such, NPs with the same surface chemistry and prepared via the same formulation process can still exhibit drastically different particle properties and biological interactions.

4.1.7. Crosslinking-Driven Self-Assembly

Finally, crosslinking processes in which polymer precipitation is driven by a crosslinking process can be used to fabricate BG-based nanoparticles. The formation of a crosslinked polymer and/or NP hydrogel network allows for both chemical stability as well as tunable pore sizes and tunable extents of swelling/water contents that can be relevant for adjusting particle mechanics, deformability, and interfacial interactions with cells.[147] For example, self-assembled curdlan NP precursors have been further crosslinked with aminated curdlan in the presence of epichlorohydrin, resulting in curdlan NP network hydrogels with hydrodynamic diameters of ≈595 nm.[132] Microgel networks have also been constructed by the crosslinking of amphiphilic methoxy PEG-grafted YBG with 3,3′-dithiodipropionic acid,[134] resulting in microgels of hydrodynamic diameters ≈300 nm and TEM (dried state) diameters of ≈75 nm consistent with the swollen nature of the microgel in aqueous suspension. Interestingly, the incorporation of redox-responsive crosslinks in this system allowed for the accelerated release of methotrexate in the presence of glutathione (90% in 96 h) relative to the absence of glutathione (60% in 96 h). Glucan hydrogels can also be prepared via photocrosslinking with other polysaccharides. For example, Kim et al.[146] demonstrated that irradiation of a solution of methacrylated SPG and hyaluronic acid (HA) functionalized with OVA via Schiff base formation in the presence of a photoinitiator followed by sonication and filtration could produce microgels that stabilized in size at ≈200 nm after 10 days, with the final microgels containing ≈3 OVA molecules per HA chain as determined by NMR. Rational choice of the crosslinker can optimize particle stability, regulate reactivity toward other polymers, and introduce stimuli-responsive degradability that may be particularly useful in a range of drug delivery applications. However, the crosslinking approach can also result in significant nanoparticle aggregation via inter-NP crosslink formation, potentially reducing particle size control; the degradability of the crosslink and its impact on any enzymatic clearance mechanism must also be considered in the context of the target application.

4.2. Immunomodulatory Applications of β-1,3 Glucan Nanoparticles

4.2.1. Cancer Immunotherapy/Drug Delivery

BG NPs have gained considerable interest in cancer therapy by leveraging their capacity for systemic administration and their high tunability of size, charge, and surface chemistry while maintaining the Dectin-1 affinity that is required for successful immune cell targeting and immunomodulation. A summary of BG NPs formulated for anti-cancer applications is shown in

Table 4. Based on their immunomodulatory properties, some BG-based nanoparticles can stimulate M1 cytokine production and reduce tumor burden in tumor-bearing mice without the co-administration of traditional chemotherapeutics; such efficacy has been demonstrated using BG-coated SPIONs[32b] as well as BG-CpG crosslinked nanogels.[148] However, it is most common to co-leverage the immunomodulatory properties of BG together with the capacity of the nanoparticle to load and deliver chemotherapeutic drugs in a single therapeutic system. Although typically designed to target and modulate MΦ, drug-loaded BG NPs can themselves have direct effects on tumor cells; for example, C26 cells treated with DOX/Zymosan NPs in vitro showed significant reductions in the mRNA expression of cancer-promoting genes via modulation of the Wnt/β-catenin signaling axis.[91a] Similarly, YBG-based NPs are well-documented to modulate MΦ mRNA and cytokine expression in vitro to alter the local inflammatory environment in a tumor. In a co-culture experiment using RAW264.7 and 4T1 cells in a transwell plate, CpG-loaded and YBG-grafted GO nanosheets induced greater 4T1 cytotoxicity compared to the controls and individual components, suggesting the combination of TLR and Dectin-1 agonists could stimulate both the production of cytokines that induce cancer cell death and increase IL-6 and TNF-α secretion in the RAW cells.[126] Interestingly, Huang et al. found that mRNA expression in RAW264.7 MΦ could be altered by tuning the YBG structure and the renaturation process of YBG/DOX NPs,[92b] with NPs prepared via pH-induced renaturation stimulating significant increases in IL-1β, IL-6, TNF-α, and IFN-γ mRNA expression whereas NPs made via DMSO-induced renaturation had no effect on IFN-γ; furthermore, low MW YBG outperformed high MW YBG in terms of both IL-1β and IFN-γ production while butyrylated YBG had no effect on mRNA expression. As such, both the chemical composition and the conformation of BG can have a significant impact on the overall bioactivity of the BG-based NP formulations, such that care must be taken to ensure the use of both relevant BG chemistries and assembly processes to achieve the desired biological activity.

There are several published examples of BG NPs exhibiting dual immunomodulatory and anti-tumoral effects in vivo across a variety of murine tumor models. Pawar et al. demonstrated that Zymosan-containing PECs could significantly reduce tumor burden in a murine breast cancer model due to its immunomodulatory properties;[105] loading of DOX into the PECs leads to a near-complete inhibition of tumor growth without any DOX-induced systemic toxicity, a result attributed to reduced $CD206^+$ MΦ and enhanced ROS/pro-inflammatory cytokine production in the tumor specifically leading to tumor cell apoptosis. Similarly, while BG alone could stimulate TNF-α and IL-12 production and increase $CD86^+$ MΦ expression against colon cancer, both activities were significantly enhanced when BG was conjugated to $BaTiO_3$ NPs, with the resulting increased T cell infiltration and ROS-induced release of DAMPs in the tumor leading to reduced tumor volume and 60% animal survival after 30 days in vivo.[128] Multimodal cancer nanotherapeutics can also be designed in which BG is one component of a multi-mechanism chemotherapeutic. For example, the benefits of chemodynamic, photothermal, and immunomodulatory effects were combined into a single system by formulating platinum/gold/YBG NPs that could significantly improve animal survival by increasing the M1/M2 MΦ ratio, promoting DC maturation, facilitating high levels of ROS/pro-inflammatory cytokines, and inducing significant apoptosis in the tumor microenvironment.[152] It is worth noting that the majority of anti-cancer BG NPs tested in vivo use YBG as the glucan source, likely due to YBG's well-known immunomodulatory capacity and its strong Dectin-1 activation compared to other glucans.[153] However, while the above examples highlight the anti-cancer efficacy of various BG nanomaterials in vivo, their effectiveness can vary significantly depending on the material design and in vivo model. For example, while the platinum/gold/YBG NPs were effective in modulating the tumor microenvironment and extending survival time, 100% mortality was still observed before 30 days likely due to the use of a clinically relevant orthotopic colon cancer model as opposed to the subcutaneous tumor model that is commonly employed. Increasing the complexity of the nanoparticle formulations can also significantly hinder ultimate clinical translation given the complexity of biological responses induced and the potential challenges in scaling up the manufacturing of such NP compositions.

4.2.2. Vaccine Formulation

Due to BG's immunostimulant properties, BG NPs are commonly designed for vaccine formulations that can combine immune cell targeting, immunomodulation, and improved antigen delivery potential, as summarized in **Table 5**. The use of NPs in vaccine formulation poses several advantages over microparticles. The small size and high surface area/volume ratio of NPs enable a greater number of surface interaction events with immune cells, enhancing ligand/receptor interactions and thus the internalization and subsequent antigen cross-presentation achievable.[154] Additionally, NPs can be prepared in sizes small enough to passively enter the lymphatic system where antigen-presenting cells (APCs) accumulate, potentially providing a more potent immune response.[155] Indeed, OVA-loaded BG NPs have demonstrated lymph node accumulation and subsequent DC activation/proliferation in multiple murine vaccination models,[102,123] inducing improved IgG titers compared to traditional alum-based adjuvants.[100,102] For example, mice infected with the EV71 virus had significantly higher anti-EV71 titers and 100% survival after 15 days when vaccinated with NPs containing carboxymethyl glucan, protamine sulfate, CpG, and inactive EV71 particles, with the enhanced response attributed to a combination of BG and CpG immunomodulatory activity.[156] In addition to vaccination efficacy, antigen-loaded BG NPs still maintain strong immunomodulatory properties; several studies have cited the induction of classic M1-like cytokines/markers in vitro and in vivo, including various interleukins, IFN-γ, iNOS, and TNF-α.[95,100,148,157] It is worth noting that these desirable adjuvancy/immunomodulatory effects can be maintained even when BG is functionalized with various functional groups including carboxyl, amino, and sulfate groups, provided sufficiently low degrees of substitution are maintained and the chain conformation of the BG is not dramatically altered.[100,114a–c]

In addition to functionalizing native BG, synthetic BG oligosaccharides have also been developed as adjuvants in murine vaccination studies; for example, a synthetic BG hexasaccharide developed by Donadei et al. directly conjugated to the

Table 4. Summary of papers describing the immunomodulatory properties of BG NPs for cancer therapy applications.

BG Material	Other NP Components	Cancer Model	Main Immunomodulatory Outcomes	Refs.
BG (carboxymethylated, phosphorylated, source not specified)	Ovalbumin, aluminum hydroxide	Murine B16-OVA tumor (in vivo)	Strong innate & adaptive immune response; 70% mouse survival over 50 days	[136]
BG (carboxymethylated, source not specified)	Protamine sulfate, CpG	Murine B16F10 tumor (in vivo)	Increased M1 markers/reduced tumor volume; further improvement with CpG present	[93]
BG from *E. gracilis*	Paclitaxel-loaded chitosan NPs	C6 & LN18 cells (in vitro)	Enhanced targeting and subsequent toxicity to C6 stem cells	[122]
Curdlan	Curcumin	HepG2 cells (in vitro)	Size- and concentration-dependent induction of reactive oxygen species and inflammatory chemokines	[140b]
Curdlan	Doxorubicin, red blood vessel vesicles	Murine A-375 tumor (in vivo)	Reduced tumor burden; increased M1/M2 MΦ ratio in tumor	[91b]
Curdlan (polyethyleneimine-grafted)	Doxorubicin, trastuzumab	Murine 4T1 tumor (in vivo)	Tumor growth inhibition even in absence of doxorubicin and trastuzumab	[149]
Laminarin	Poly(ethylene glycol)-poly(lactic acid) polymersomes	Murine B16F10 tumor (in vivo)	Immune cell proliferation; reduced tumor burden across multiple treatment models	[141]
Not specified	Superparamagnetic iron oxide NPs	Murine CT-26 liver tumor (in vivo)	Targeting and accumulation in liver macrophages for magnetic resonance imaging	[118]
Schizophyllan	CpG, ovalbumin	Murine E.G7-OVA tumor (in vivo)	Increased IL-6 production; reduced tumor burden; improved survival	[148]
YBG	Zn/doxorubicin complexes	Murine AK4.4 pancreatic cancer (in vivo)	Increased M1/M2 MΦ ratio & infiltrating T cells in tumor	[131]
YBG	Ferumoxytol	Murine B16F10 tumor (in vivo)	Reduced tumor burden; increased M1/M2 MΦ ratio in tumor	[32b]
YBG	$CaCO_3$ NPs	Murine H22 lymph node metastasis (in vivo)	Increased M1/M2 MΦ & cytokine ratio in both primary tumor and metastatic lymph nodes	[130]
YBG	Doxorubicin	RAW 264.7 cells (in vitro)	Significant increase in M1 mRNA expression depending on YBG MW and functionalization	[92b]
YBG	CpG, graphene oxide nanosheet	RAW264.7/4T1 co-culture (in vitro)	Enhanced IL-6 & TNF-α secretion when all 3 components are present	[126]
YBG (decylamine-conjugated)	Capric acid, citric acid, sodium bicarbonate, paclitaxel	Orthotopic DSL-6A/C1 tumor (in vivo)	Enhanced DC maturation and significant reduction in tumor burden when coated with BG	[150]
YBG (low MW)	Doxorubicin or temozolomide prodrug	Murine ALTS1C1 or LCPN brain tumor (in vivo)	Enhanced tumor accumulation compared to free drug; 100% survival over 30 days	[143]
YBG (low MW)	$BaTiO_3$ NPs	Murine CT-26 tumor (in vivo)	Elevated reactive oxygen species production, T cell infiltration, & reduced tumor burden	[128]
YBG (ultrasound fragmented)	QMC12 photosensitizer	Murine B16 tumor (in vivo)	100% primary tumor inhibition when combined with αPD-L1 therapy	[151]
YBG (ultrasound fragmented)	Gold & platinum NPs	Murine B16F10 tumor (in vivo)	Significant increase in M1/M2 ratio in tumors; increased DC, T cell, and MΦ infiltration; improved survival	[152]
Zymosan (hydrolyzed)	Doxorubicin	C26 cells (in vitro)	Reduced expression of Wnt/β-catenin axis genes; synergistic cytotoxicity with doxorubicin	[91a]
Zymosan (low MW)	mRNA, lipid NPs	Murine E.G7-OVA tumor (in vivo)	Enhanced DC maturation/T cell proliferation; 40% complete tumor regression	[145]
Zymosan (oxidized)	mRNA, lipid nanoparticles	Murine E.G7-OVA tumor (in vivo)	BG-dependent DC maturation in vivo	[145]
Zymosan (sulfated)	Doxorubicin, poly(ethylene glycol)-*b*-polyethyleneimine	Murine 4T1 tumor (in vivo)	Increased M1 MΦ and apoptosis in tumor; reduced tumor burden	[105]

Table 5. Summary of papers describing the immunomodulatory properties of BG NPs for non-cancer applications.

BG Material	Other NP Components	Application	Biological Model	Main Immunomodulatory Outcomes	Refs.
Schizophyllan (methacrylated)	Methacrylated hyaluronic acid, ovalbumin	Dermal delivery to DCs	Porcine skin penetration (ex vivo); JAWSII cells	Enhanced DC maturation when schizophyllan present	[146]
YBG (3-boronobenzoic acid modified)	Chitosan, phycocyanin, lutein	Eye disease	RAW264.7 (in vitro); Murine dry eye model (in vivo)	Promotion of M1 phenotype; reduced eye inflammation in vivo	[99]
Curdlan (aminated); curdlan NPs	Epichlorohydrin crosslinker	Gene delivery	THP-1 MΦ	Dectin-1-mediated uptake; shift toward M1 mRNA expression	[132]
YBG (aminated)	pDNA	Gene delivery	RAW264.7 MΦ	Inhibition of M1 mRNA in LPS-stimulated MΦ	[101]
YBG (soluble)	Selenium NPs	Immuno-suppression prevention	Murine cyclophosphamide-induced immunosuppression	Replenishment of immune cell counts and increased M1 markers in vivo	[119a]
BG from *E. gracilis*	PLGA NPs, chitosan, rifampicin	Infectious diseases	Human alveolar-like MΦ	Increased reactive oxygen species, M1 cytokine levels in vitro	[120]
Curdlan	Poly(lactic-co-glycolic acid) NPs	Infectious diseases	*M. tuberculosis*-infected RAW264.7 cells	Curdlan-induced TNF-α secretion; no reduction in bacterial burden	[158]
Curdlan (sulfated)	Chitosan, rifampicin, D-pinitol	Infectious diseases	*M. smegmatis*-infected RAW264.7 cells	Significant increase in M2/M1 mRNA ratio	[96]
YBG (oxidized)	Cefotaxime prodrug	Infectious diseases	Murine meningitis model (in vivo)	Reduction in bacteria-induced inflammatory cytokines/chemokines	[144]
YBG (soluble)	Polystyrene NPs	Infectious diseases	*C. albicans*-infected bone marrow-derived DCs	Reduced inflammatory response when pre-treated with BG NPs	[127a]
YBG (acetylated)	Polydopamine	Inflammatory bowel disease	Murine acute colitis model	Reduced inflammatory markers; gut microbiome modulation	[142]
Curdlan (aminated)	Fullerene	Liver disease	Murine autoimmune hepatitis	Reduced NF-κB activity and apoptosis in liver	[125a]
BG (sulfated) from *H. erinaceus*	Chitosan, resveratrol	MΦ modulation (general)	RAW264.7 cells	Reduced inflammatory cytokine release via regulation of several signalling pathways	[94]
BG from *Pleurotus tuber-regium*	Superparamagnetic iron oxide NPs	MΦ modulation (general)	Bone marrow-derived MΦ	Increased reactive oxygen species, M1 cytokine/NF-κB gene expression	[135]
Curdlan	Poly(γ-glutamic acid)	MΦ modulation (general)	Monocyte-derived MΦ	Significant increase in several M1 markers compared to free curdlan	[139]
Curdlan	Tween 80	MΦ modulation (general)	Peripheral blood mononuclear cells, RAW264.7 cells	Size-dependent production of reactive oxygen species/M1 cytokines	[140a]
YBG (oxidized)	CpG-loaded glycogen NPs	MΦ modulation (general)	RAW264.7 cells	Enhanced uptake, M1 cytokine secretion in vitro	[103]
YBG	Methoxy-PEG, methotrexate	Periodontal bone regeneration	Murine LPS-induced periodontitis model	Increased M2/M1 MΦ ratio; bone regeneration in vivo	[159]
YBG	Methoxy-PEG, methotrexate	Rheumatoid arthritis therapy	Murine collagen-induced arthritis	Increased M2/M1 MΦ ratio; reduced M1 mRNA when drug present	[134]
BG (aminated)	CpG; ovalbumin	Vaccination	Murine ovalbumin vaccination	Significantly higher IgG, IFN-γ, IL-4 compared to alum	[100]
BG (carboxylated)	Mesoporous silica NPs, ovalbumin	Vaccination	Murine ovalbumin vaccination	Lymph node targeting & DC activation in vivo	[123]
BG (carboxymethylated)	Protamine sulfate; CpG; enterovirus	Vaccination	Murine EV71 virus challenge	Strong increase in IFN-γ; 100% survival 15 days post-challenge	[156]
Curdlan (carboxymethylated)	Chitosan chloride; *N*-trimethyl chitosan; bovine serum albumin	Vaccination	Murine nasal/subcutaneous vaccination	Increased M1 cytokines, IgG titres 253 days after priming dose	[95]
Curdlan (sulfated)	Quaternary ammonium-modified chitosan, SARS-CoV-2 spike receptor binding domain	Vaccination	Murine nasal vaccination	Improved IgG titres and pro-inflammatory cytokine secretion compared to traditional adjuvants	[98]
Curdlan (sulfated)	Trimethyl chitosan; ovalbumin	Vaccination	Peritoneal MΦ; bone marrow DCs	Strong induction of M1 cytokines/metabolites; DC maturation in vitro	[157]
Schizophyllan	CpG; ovalbumin	Vaccination	Murine intradermal vaccination	Increased IL-6 & $CD8^+$ T cells when crosslinked schizophyllan present	[148]

(*Continued*)

Table 5. (Continued)

BG Material	Other NP Components	Application	Biological Model	Main Immunomodulatory Outcomes	Refs.
Schizophyllan	CpG; ovalbumin	Vaccination	Murine E.G17-OVA cancer vaccination	80% reduction in cancer cells when mice were pre-immunized	[107b]
Synthetic BG hexasaccharide	CRM_{197} antigen	Vaccination	Murine intramuscular/intradermal vaccination	Strong Dectin-1 affinity; comparable adjuvant performance to alum	[160]
YBG (carboxy-methylated)	Chitosan; ovalbumin	Vaccination	Murine ovalbumin vaccination	Lymph node accumulation; DC proliferation; increased IgG titres compared to alum	[102]
YBG (soluble)	Poly[2-(dimethylamino) ethylmethacrylate]/poly(β-amino ester)/DNA complex	Vaccination	Murine subcutaneous vaccination	Improved transfection in vitro; no improvement in IgG titres in vivo	[121a]
YBG	PLGA NPs	Vaccination; trained immunity	Murine training model; B16F10 & EG7.OVA tumor models	Slow release of YBG improved MΦ training, and tumor burden compared to free YBG	[161]

CRM_{197} antigen was demonstrated to promote strong Dectin-1 binding affinity while providing similar adjuvancy effects to those of alum.[160] The well-defined hexasaccharide structure is of particular relevance for producing conjugates with controlled ligand density and structure, potentially yielding more predictable biological responses in vivo relative to polymeric BG that can alter its conformation depending on the assembly technique used for NP formulation and/or the polymer/NP microenvironment.

4.2.3. Other Immunomodulatory Applications

As shown in Table 5, BG NPs can be prepared to improve the treatment of a wide variety of other target diseases and applications, with BG NPs having been noted to be particularly well-suited for treating macrophage-targeted bacterial infections. However, the immunomodulatory effects of BG in this context are inconsistent in the literature. For example, BG-coated rifampicin-loaded NPs have been shown to induce high levels of intracellular ROS as well as enhanced TNF-α, IFN-γ, and IL12-p70 production in human alveolar-like MΦ, all of which are important components of the bacterial infection response.[120] TNF-α secretion has also been reported in *M. tuberculosis*-infected RAW264.7 cells, although no significant improvement in bacterial burden was observed in vitro.[158] Conversely, multiple in vitro and in vivo studies have shown that BG NPs can significantly reduce phagocytic activity and inflammatory cytokine secretion to result in improved bacterial killing.[96,127a,144] However, many of these examples do not distinguish between the immunomodulatory effects of BG and the loaded therapeutic that may promote contradictory biological effects.[96,144]

Such contradictory biological indications are particularly evident in examples in which BG NPs are combined with other NP agents or bioactives that aim to induce anti-inflammatory properties useful for treating diseases including hepatitis and rheumatoid arthritis. In such cases, the BG component is typically employed to enable macrophage targeting while the observed anti-inflammatory effect is induced primarily by the other NP components; in this context, while BGs have demonstrated a propensity to reprogram MΦ toward a pro-inflammation M1-like polarization state, the drug used in the formulation has a stronger anti-inflammatory effect to control the overall inflammatory response. In a murine autoimmune hepatitis model, curdlan-conjugated fullerene exhibited anti-inflammatory effects without the inclusion of additional drugs, with significant reductions in inflammatory cytokines and lowered white blood cell and neutrophil counts achieved that led to reduced apoptosis in murine liver tissues.[125a] In a murine arthritis model, methotrexate-loaded YBG-PEG NPs significantly reduced the mRNA levels of several inflammatory cytokines while also shifting the M1/M2 ratio toward an M2-dominant phenotype; in contrast, when only YBG-PEG was present without the drug, these effects were less pronounced and an M1-dominant phenotype was maintained.[134] Finally, in a murine acute colitis model, polydopamine-coated YBG NPs effectively reduced inflammatory markers in the colon to improve body weight recovery, promote probiotic bacteria proliferation, and reduce the levels of bacteria implicated in inflammatory bowel disease;[142] in this case, the antioxidant/anti-inflammatory properties of polydopamine were primarily associated with the reduced inflammatory state, although the uncoated particles were also effective in lowering TNF-α and IL-1β levels. Thus, the comparatively modest pro-inflammatory response but consistently strong MΦ-targeting ability of BGs can be used to improve the localization of bioactive drugs or materials that can induce strong both pro- or anti-inflammatory responses.

5. Conclusion and Future Outlook

The diverse structures and ease of functionalization of BG allow for the fabrication of microparticles and nanoparticles with tunable sizes, morphologies, and immunomodulatory effects, either alone or in combination with additional therapeutics to target a wide range of immune-dysregulated diseases. However, the large variations in both composition and conformation across different BG materials result in inconsistent biological effects being reported across the literature depending on the chemical composition, molecular weight, and morphology of the BG used. Interpreting biological responses is further complicated by the differences in macrophage/DC phenotypes across various in vitro and in vivo models. Thus, future work on therapeutic BG particles should focus on the following aspects:

1) *Improving the physicochemical characterization of BG materials*: BG properties vary widely across different sources but can also exhibit significant batch-to-batch variation even from a single source. It is thus important to consistently distinguish these differences at both the polymer level, at which properties like molecular weight and chain conformation will impact Dectin-1 binding affinity and activation, and the particle level, at which variations in particle size, morphology, and surface chemistry will influence the ability to target immune cells, cluster and activate surface receptors, and enter cells to deliver payloads. As noted several times in this review, a significant fraction of papers that report the utility of BG-based therapeutics do not report the source of the BG or how the BG was (or was not) processed prior to testing; without such information, it is not possible to develop the required structure-property relationships to better predict BG's immunomodulatory activity, as is necessary for rational utilization of BG in the clinic.
2) *Improving the purification of BG*: The purity of BG can have a significant effect on its resulting immunomodulatory properties. For example, Zymosan, an impure form of YBG, is a strong TLR activator in addition to its Dectin-1 affinity, leading to biological responses that are difficult to compare with other purified BG materials. Increased emphasis should thus be placed on either rigorously removing such impurities via extraction or other emerging techniques (e.g., supercritical fluid processing) or rigorously characterizing the concentration and chemistry of the impurities, as the presence of those impurities may in some cases be beneficial to either upregulate or suppress the degree of immunomodulation imparted by BG alone depending on the biological activity targeted.
3) *Improving our understanding of the effect of BG functionalization on biological activity*: While several examples in this review highlight the immunomodulatory activities of a variety of BG derivatives, minimal research effort has been invested in systematically investigating how the type of functional group and/or the degree of functionalization of BG affect the extent of immunomodulation possible. For example, it has been demonstrated that the introduction of charged functional groups can alter BG chain conformation in solution and thus receptor binding affinity and downstream effects like anticancer activity.[162] While BG functionalization can introduce the potential to fabricate a host of new polymeric or nanoscale structures, better understanding the effect of that modification chemistry on bioactivity (particularly Dectin-1 binding and activation) would ensure that optimal solubilization techniques and/or assembly techniques are chosen to maximize the maintenance of BG bioactivity in a particular application.
4) *Improving the biological context of BG validation experiments*: Most BG studies use either macrophage-derived cell lines or primary monocytes/macrophages recovered from animal models to probe BG immunomodulatory responses in 2D cell culture. While the use of cell lines in this context can have benefits in terms of reproducing the performance metrics of various BG derivatives between labs, 2D models of macrophage or macrophage-derived cells omit the rest of the biological context of real tissues and thus cannot always predict the multi-faceted responses of real tissues to BG. Advanced 3D tissue models in which macrophages are one component (e.g., cancer spheroids combining cancer cells, fibroblasts, and macrophages)[163] and/or expanded use of ex vivo methods like precision cut tissue slices from the target tissue (in which one animal tissue can provide many test slices in which macrophages can be interrogated within their full native biological milieu) should thus be emphasized to better predict BG responses prior to in vivo experimentation (or understand any inconsistent responses observed in vivo).
5) *Designing improved micro/nanostructures from BG-based materials to enhance therapeutic activity*: Coupling the immunomodulatory activity of BG with intelligent particle design offers the potential for site-specific immunomodulation and drug delivery to improve therapeutic outcomes while minimizing off-target effects. For example, better leveraging YBG's size and porosity to develop inhalable delivery vehicles/therapeutics that can access deeper into the lung for treating fibrosis, developing glucan shell-protected NPs to promote drug delivery within the gastrointestinal tract, and designing nanoparticles enabling prolonged circulation times and/or site-specific exposure of BG in the target microenvironment (e.g., to present the glucan ligand only to macrophages at the disease site to minimize off-target immunomodulatory effects) all represent opportunities to improve the clinical efficacy of BG therapies while reducing potential side effects.

Acknowledgements

The authors thank the Natural Sciences and Engineering Research Council of Canada (NSERC, Collaborative Health Research Partnerships Grant CHRPJ-538813-2019 to TH), the Canadian Institutes of Health Research (CIHR, Collaborative Health Research Partnerships Grant CPG -163975 to TH), Mitacs Canada (Accelerate Grants IT18595 and IT29330 to TH), and the Ontario Graduate Scholarship Program (to ND) for funding.

Conflict of Interest

The authors declare no conflict of interest.

Keywords

beta-glucan, drug delivery, immunomodulation, macrophages, microparticles, nanoparticles

Received: February 23, 2025
Revised: April 17, 2025
Published online: April 29, 2025

[1] J. Lichtnekert, T. Kawakami, W. C. Parks, J. S. Duffield, *Curr. Opin. Pharmacol.* **2013**, *13*, 555.
[2] D. S. Vinay, E. P. Ryan, G. Pawelec, W. H. Talib, J. Stagg, E. Elkord, T. Lichtor, W. K. Decker, R. L. Whelan, H. S. Kumara, *Semin. Cancer Biol* **2015**.
[3] S. Ostrand-Rosenberg, P. Sinha, D. W. Beury, V. K. Clements, *Semin. Cancer Biol* **2012**.
[4] a) W.-C. Zhou, Q.-B. Zhang, L. Qiao, *World J. Gastroenterol.* **2014**, *20*, 7312; b) A. K. Ghosh, S. E. Quaggin, D. E. Vaughan, *Exp. Biol. Med.*

2013, *238*, 461; c) F. J. Martinez, H. R. Collard, A. Pardo, G. Raghu, L. Richeldi, M. Selman, J. J. Swigris, H. Taniguchi, A. U. Wells, *Nat. Rev. Disease Primers* **2017**, *3*, 1.
[5] a) J. P. Finnerty, A. Ponnuswamy, P. Dutta, A. Abdelaziz, H. Kamil, *BMC Pulm. Med.* **2021**, *21*, 411; b) T. Ogura, H. Taniguchi, A. Azuma, Y. Inoue, Y. Kondoh, Y. Hasegawa, M. Bando, S. Abe, Y. Mochizuki, K. Chida, *Eur. Respir. J.* **2015**, *45*, 1382; c) L. Wollin, E. Wex, A. Pautsch, G. Schnapp, K. E. Hostettler, S. Stowasser, M. Kolb, *Eur. Respir. J.* **2015**, *45*, 1434.
[6] J. A. Hubbell, S. N. Thomas, M. A. Swartz, *Nature* **2009**, *462*, 449.
[7] D. Li, M. Wu, *Signal Transduction Targeted Ther.* **2021**, *6*, 291.
[8] a) Food & Drug Administration, *GRN No. 239 Bakers yeast beta-glucan*, https://www.hfpappexternal.fda.gov/scripts/fdcc/index.cfm?set=GRASNotices&id=239&sort=GRN_No&order=DESC&startrow=1&type=basic&search=239 (accessed: April 2025); b) Food & Drug Administration, *GRN No. 309 Beta-glucan derived from Aureobasidium pullulans*, https://www.hfpappexternal.fda.gov/scripts/fdcc/index.cfm?set=grasnotices&id=309&sort=GRN_No&order=DESC&startrow=1&type=basic&search=309 (accessed: April 2025); c) Food & Drug Administration, *GRN No. 997 Chitosan and beta-1,3-glucans from white button mushrooms (Agaricus bisporus)*, https://hfpappexternal.fda.gov/scripts/fdcc/index.cfm?set=GRASNotices&id=997&sort=GRN_No&order=DESC&startrow=1&type=basic&search=997 (accessed: April 2025).
[9] J. Richter, V. Svozil, V. Král, L. R. Dobiášová, I. Stiborová, V. Vetvicka, *Ann. Transl. Med.* **2014**, *2*, 15.
[10] M. Muroya, K. Nakada, K. Maruo, K. Hashimoto, *Eur. J. Clin. Nutr.* **2025**, 1.
[11] I. Y. Cheung, A. Mauguen, S. Modak, G. Ragupathi, E. M. Basu, S. S. Roberts, B. H. Kushner, N.-K. Cheung, *JAMA Oncol.* **2023**, *9*, 242.
[12] A. B. Weitberg, *J. Exp. Clin. Cancer Res.* **2008**, *27*, 1.
[13] P. Kanjan, N. M. Sahasrabudhe, B. J. de Haan, P. de Vos, *J. Funct. Foods* **2017**, *37*, 433.
[14] H. S. Goodridge, C. N. Reyes, C. A. Becker, T. R. Katsumoto, J. Ma, A. J. Wolf, N. Bose, A. S. Chan, A. S. Magee, M. E. Danielson, *Nature* **2011**, *472*, 471.
[15] Z. Zheng, Q. Huang, Y. Kang, Y. Liu, W. Luo, *Carbohydr. Polym.* **2021**, *273*, 118568.
[16] M. McIntosh, B. Stone, V. Stanisich, *Appl. Microbiol. Biotechnol.* **2005**, *68*, 163.
[17] S. M. V. Mejía, A. de Francisco, B. Bohrer, *Crit. Rev. Food Sci. Nutr.* **2020**, *60*, 3693.
[18] R. Zhang, K. J. Edgar, *Biomacromolecules* **2014**, *15*, 1079.
[19] C. Borchani, F. Fonteyn, G. Jamin, J. Destain, L. Willems, M. Paquot, C. Blecker, P. Thonart, *Crit. Rev. Food Sci. Nutr.* **2016**, *56*, 1746.
[20] J. Chen, R. Seviour, *Mycol. Res.* **2007**, *111*, 635.
[21] M. Novak, V. Vetvicka, *J. Immunotoxicol.* **2008**, *5*, 47.
[22] Y. Meng, F. Lyu, X. Xu, L. Zhang, *Biomacromolecules* **2020**, *21*, 1653.
[23] F. Zhu, B. Du, B. Xu, *Food Hydrocolloids* **2016**, *52*, 275.
[24] L. Pillemer, E. Ecker, *J. Biol. Chem.* **1941**, *137*, 139.
[25] Z. Rao, Y. Dong, X. Zheng, K. Tang, J. Liu, *Biocatal. Agric. Biotechnol.* **2021**, *37*, 102163.
[26] Y. Zhang, H. Kong, Y. Fang, K. Nishinari, G. O. S. Phillips, *Bioact. Carbohydr. Diet. Fibre* **2013**, *1*, 53.
[27] a) R. Di Paola, E. Mazzon, T. Genovese, C. Crisafulli, P. Bramanti, R. Caminiti, E. Esposito, M. P. Fink, S. Cuzzocrea, *Crit. Care Med.* **2009**, *37*, 270; b) D. L. Williams, *Mediat. Inflamm.* **1997**, *6*, 247.
[28] K. Ariizumi, G.-L. Shen, S. Shikano, S. Xu, R. Ritter, T. Kumamoto, D. Edelbaum, A. Morita, P. R. Bergstresser, A. Takashima, *J. Biol. Chem.* **2000**, *275*, 20157.
[29] G. D. Brown, S. Gordon, *Nature* **2001**, *413*, 36.
[30] a) D. M. Reid, N. A. Gow, G. D. Brown, *Curr. Opin. Immunol.* **2009**, *21*, 30; b) C. Lee, R. Verma, S. Byun, E.-J. Jeun, G.-C. Kim, S. Lee, H.-J. Kang, C. J. Kim, G. Sharma, A. Lahiri, *Nat. Commun.* **2021**, *12*, 3611; c) G. D. Brown, J. Herre, D. L. Williams, J. A. Willment, A. S. Marshall, S. Gordon, *J. Exp. Med.* **2003**, *197*, 1119.
[31] a) Z.-J. Xu, Y. Gu, C.-Z. Wang, Y. Jin, X.-M. Wen, J.-C. Ma, L.-J. Tang, Z.-W. Mao, J. Qian, J. Lin, *Oncoimmunology* **2020**, *9*, 1683347; b) T. Rőszer, *Mediators Inflammation* **2015**, 2015.
[32] a) M. Liu, F. Luo, C. Ding, S. Albeituni, X. Hu, Y. Ma, Y. Cai, L. McNally, M. A. Sanders, D. Jain, *J. Immunol.* **2015**, *195*, 5055; b) X. Liu, Y. Xu, Y. Li, Y. Pan, S. Zhao, Y. Hou, *Int. J. Med. Sci.* **2021**, *18*, 3125; c) P. de Graaff, C. Berrevoets, C. Rösch, H. A. Schols, K. Verhoef, H. J. Wichers, R. Debets, C. C. Govers, *Cancer Immunol., Immunother* **2021**, *70*, 547.
[33] B. Li, Y. Cai, C. Qi, R. Hansen, C. Ding, T. C. Mitchell, J. Yan, *Clin. Cancer Res.* **2010**, *16*, 5153.
[34] J. Ding, Y. Ning, Y. Bai, X. Xu, X. Sun, C. Qi, *Med. Microbiol. Immunol.* **2019**, *208*, 39.
[35] a) J. A. Champion, A. Walker, S. Mitragotri, *Pharm. Res.* **2008**, *25*, 1815; b) Y. Tabata, Y. Ikada, *Biomaterials* **1988**, *9*, 356.
[36] a) P. Muttil, J. Kaur, K. Kumar, A. B. Yadav, R. Sharma, A. Misra, *Eur. J. Pharm. Sci.* **2007**, *32*, 140; b) E. Soto, Y. S. Kim, J. Lee, H. Kornfeld, G. Ostroff, *Polymers* **2010**, *2*, 681.
[37] D. S. Kohane, *Biotechnol. Bioeng.* **2007**, *96*, 203.
[38] H. Jain, A. Bairagi, S. Srivastava, S. B. Singh, N. K. Mehra, *Drug Discovery Today* **2020**, *25*, 1865.
[39] a) G. Mocanu, D. Mihai, M. Moscovici, L. Picton, D. LeCerf, *Int. J. Biol. Macromol.* **2009**, *44*, 215; b) I. Popescu, I. M. Pelin, M. Butnaru, G. Fundueanu, D. M. Suflet, *Carbohydr. Polym.* **2013**, *94*, 889.
[40] a) C. Liu, P. C. Cheung, *J. Agric. Food Chem.* **2019**, *67*, 9070; b) C. F. Ellefsen, A.-M. Struzek, R. Scherließ, M. Hiorth, A. B. C. Samuelsen, *ACS Appl. Bio Mater.* **2023**, *6*, 1863; c) Z. Liu, L. Yu, P. Gu, R. Bo, A. Wusiman, J. Liu, Y. Hu, D. Wang, *Carbohydr. Polym.* **2020**, *245*, 116520.
[41] J. Yan, D. J. Allendorf, B. Brandley, *Expert Opin. Biol. Ther.* **2005**, *5*, 691.
[42] a) Y. Wang, S. Yao, T. Wu, *World J. Microbiol. Biotechnol.* **2003**, *19*, 947; b) M. Magnani, C. M. Calliari, F. C. de Macedo Jr, M. P. Mori, I. M. de Syllos Cólus, R. J. Castro-Gomez, *Carbohydr. Polym.* **2009**, *78*, 658.
[43] Z. Hromádková, A. Ebringerová, V. Sasinková, J. Šandula, V. Hříbalová, J. Omelková, *Carbohydr. Polym.* **2003**, *51*, 9.
[44] a) X.-Y. Liu, Q. Wang, S. W. Cui, H.-Z. Liu, *Food Hydrocolloids* **2008**, *22*, 239; b) K. W. Hunter, R. A. Gault, M. D. Berner, *Lett. Appl. Microbiol.* **2002**, *35*, 267.
[45] a) V. Petravić-Tominac, V. Zechner-Krpan, K. Berković, P. Galović, Z. Herceg, S. Srečec, I. Špoljarić, *Food Technol. Biotechnol.* **2011**, *49*, 56; b) V. Zechner-Krpan, V. Petravić-Tominac, I. Gospodarić, L. Sajli, S. Đaković, J. Filipović-Grčić, *Food Technol. Biotechnol.* **2010**, *48*, 189; c) V. Zechner-Krpan, V. Petravić-Tominac, P. Galović, V. Galović, J. Filipović-Grčić, S. Srečec, *Agric. Conspec. Sci.* **2010**, *75*, 45.
[46] a) K. Makino, N. Yamamoto, K. Higuchi, N. Harada, H. Ohshima, H. Terada, *Colloids Surf., B* **2003**, *27*, 33; b) T. Hasegawa, K. Hirota, K. Tomoda, F. Ito, H. Inagawa, C. Kochi, G.-I. Soma, K. Makino, H. Terada, *Colloids Surf., B* **2007**, *60*, 221.
[47] a) Y. Xie, S. Jiang, F. Xia, X. Hu, H. He, Z. Yin, J. Qi, Y. Lu, W. Wu, *J. Mater. Chem. B* **2016**, *4*, 4040; b) G. Ruphuy, I. Salon, J. Tomas, P. Salamunova, J. Hanus, F. Stepanek, *Int. J. Pharm.* **2020**, *576*, 118990.
[48] D. Heng, S. H. Lee, W. K. Ng, R. B. Tan, *Expert Opin. Drug Delivery* **2011**, *8*, 965.
[49] a) K. Cal, K. Sollohub, *J. Pharm. Sci.* **2010**, *99*, 575; b) S. Poozesh, E. Bilgili, *Int. J. Pharm.* **2019**, *562*, 271.
[50] P. Šalamúnová, I. Saloň, G. Ruphuy, J. Kroupová, M. Balouch, J. Hanuš, F. Štěpánek, *Eur. J. Pharm. Biopharm.* **2021**, *168*, 15.

[51] P. Šalamúnová, L. Cupalová, M. Majerská, J. Treml, G. Ruphuy, K. Šmejkal, F. Štěpánek, J. Hanuš, J. Hošek, *Int. J. Biol. Macromol.* **2021**, *169*, 443.
[52] a) A. Sosnik, K. P. Seremeta, *Adv. Colloid Interface Sci.* **2015**, *223*, 40; b) M.-I. Ré, *Drying Technol.* **2006**, *24*, 433.
[53] E. Dadkhodazade, A. Mohammadi, S. Shojaee-Aliabadi, A. M. Mortazavian, L. Mirmoghtadaie, S. M. Hosseini, *Food Biophys.* **2018**, *13*, 404.
[54] F. Ahmad, S. Ahmad, T. K. Upadhyay, S. Singh, M. Khubaib, J. Singh, M. Saeed, I. Ahmad, L. A. Al-Keridis, R. Sharma, *Sci. Rep.* **2024**, *14*, 16437.
[55] W. Wang, *Int. J. Pharm.* **2000**, *203*, 1.
[56] I. Saloň, J. Hanuš, P. Ulbrich, F. Štěpánek, *Food Bioprod. Process.* **2016**, *99*, 128.
[57] a) K. Lee, Y. Kwon, J. Hwang, Y. Choi, K. Kim, H.-J. Koo, Y. Seo, H. Jeon, J. Choi, *ACS Omega* **2019**, *4*, 668; b) D. Rotrekl, B. Devriendt, E. Cox, L. Kavanová, M. Faldyna, P. Šalamúnová, Z. Bačo, V. Prokopec, F. Štěpánek, J. Hanuš, J. Hošek, *Int. J. Pharm.* **2020**, *582*, 119318; c) Y. Sun, B. Duan, H. Chen, X. Xu, *Adv. Healthcare Mater.* **2020**, 9.
[58] a) X. Zhang, Y. Zhao, Y. Xu, Y. Pan, F. Chen, A. Kumar, G. Zou, X. J. Liang, *J. Mater. Chem. B* **2014**, *2*, 5882; b) H. Huang, G. R. Ostroff, C. K. Lee, C. A. Specht, S. M. Levitz, *MBio* **2010**, *1*.
[59] a) E. R. Soto, A. C. Caras, L. C. Kut, M. K. Castle, G. R. Ostroff, *J. Drug Delivery* **2012**, *2012*, 1; b) E. R. Soto, O. O'Connell, F. Dikengil, P. J. Peters, P. R. Clapham, G. R. Ostroff, *J. Drug Delivery* **2016**, *2016*, 1; c) X. Zhou, X. Zhang, S. Han, Y. Dou, M. Liu, L. Zhang, J. Guo, Q. Shi, G. Gong, R. Wang, J. Hu, X. Li, J. Zhang, *Nano Lett.* **2017**, *17*, 1056; d) T. Ren, J. Gou, W. Sun, X. Tao, X. Tan, P. Wang, Y. Zhang, H. He, T. Yin, X. Tang, *Mol. Pharmaceutics* **2018**, *15*, 2870; e) Z. Hamza, M. El-Hashash, S. Aly, A. Hathout, E. Soto, B. Sabry, G. Ostroff, *Carbohydr. Polym.* **2019**, *203*, 185; f) X. Zhou, K. Ling, M. Liu, X. Zhang, J. Ding, Y. Dong, Z. Liang, J. Li, J. Zhang, *Theranostics* **2019**, *9*, 6568; g) T. Ren, X. Zheng, R. Bai, Y. Yang, L. Jian, *Int. J. Pharm.* **2021**, *601*, 120583; h) X. Han, R. Luo, S. Qi, Y. Wang, L. Dai, W. Nie, M. Lin, H. He, N. Ye, C. Fu, *J. Nanobiotechnol.* **2023**, *21*, 321.
[60] R. Bastos, P. G. Oliveira, V. M. Gaspar, J. F. Mano, M. A. Coimbra, E. Coelho, *Carbohydr. Polym.* **2022**, *277*, 118826.
[61] F. Sahena, I. Zaidul, S. Jinap, A. Karim, K. Abbas, N. Norulaini, A. Omar, *J. Food Eng.* **2009**, *95*, 240.
[62] a) B. Díaz-Reinoso, A. Moure, H. Domínguez, J. C. Parajó, *J. Agric. Food Chem.* **2006**, *54*, 2441; b) F. Rindfleisch, T. P. DiNoia, M. A. McHugh, *J. Phys. Chem.* **1996**, *100*, 15581.
[63] N. Carrigy, R. Vehring, in *Pharmaceutical Inhalation Aerosol Technology*, 3rd ed., CRC Press, Boca Raton **2019**, p. 291.
[64] a) Ó. Benito-Román, E. Alonso, M. J. Cocero, M. Goto, *Food Bioprod. Process* **2016**, *98*, 21; b) N. Liu, R. Couto, B. Seifried, P. Moquin, L. Delgado, F. Temelli, *Food Res. Int.* **2018**, *106*, 354; c) K.-a. Johnson, N. Muzzin, S. Toufanian, R. A. Slick, M. W. Lawlor, B. Seifried, P. Moquin, D. Latulippe, T. Hoare, *Acta Biomater.* **2020**, *112*, 101; d) D. A. Osorio, B. Seifried, P. Moquin, K. Grandfield, E. D. Cranston, *J. Mater. Sci.* **2018**, *53*, 9842; e) J. R. Barbosa, M. M. S. Freitas, L. C. Oliveira, L. H. S. Martins, A. O. Almada-Vilhena, R. M. Oliveira, J. C. Pieczarka, B. Davi do Socorro, R. N. C. Junior, *Food Chem.* **2020**, *330*, 127173.
[65] M. Salgado, F. Santos, S. Rodríguez-Rojo, R. L. Reis, A. R. C. Duarte, M. J. Cocero, *J. CO2 Util.* **2017**, *22*, 262.
[66] C. Errenst, M. Petermann, A. Kilzer, *J. Supercrit. Fluids* **2021**, *168*, 105076.
[67] S. Naiel, N. Dowdall, Q. Zhou, P. Ali, A. Hayat, M. Vierhout, E. Wong, R. Couto, B. Yepez, B. Seifried, P. Moquin, M. R. Kolb, K. Ask, T. Hoare, *Biomaterials* **2025**, *313*, 122816.
[68] H. Huang, G. R. Ostroff, C. K. Lee, J. P. Wang, C. A. Specht, S. M. Levitz, *Infect. Immun.* **2009**, *77*, 1774.
[69] Z. Zhu, L. He, Y. Bai, L. Xia, X. Sun, C. Qi, *Clin. Exp. Immunol.* **2023**, *214*, 50.
[70] C. Y. Perrot, T. Karampitsakos, J. D. Herazo-Maya, *Am. J. Physiol. Cell Physiol.* **2023**, *325*, C1046.
[71] a) J. W. van der Meer, L. A. Joosten, N. Riksen, M. G. Netea, *Mol. Immunol.* **2015**, *68*, 40; b) V. P. Mourits, J. C. Wijkmans, L. A. Joosten, M. G. Netea, *Curr. Opin. Pharmacol.* **2018**, *41*, 52.
[72] a) B. G. J. Moerings, P. d. Graaff, M. Furber, R. F. Witkamp, R. Debets, J. J. Mes, J. v. Bergenhenegouwen, C. Govers, *Front. Immunol.* **2021**, 12; b) C. Ding, R. Shrestha, X. Zhu, A. E. Geller, S. Wu, M. R. Woeste, W. Li, H. Wang, F. Yuan, R. Xu, *Nat. Immunol.* **2023**, 1.
[73] S. J. Moorlag, N. Khan, B. Novakovic, E. Kaufmann, T. Jansen, R. van Crevel, M. Divangahi, M. G. Netea, *Cell Rep.* **2020**, 31.
[74] S. Jamas, C. Rha, A. J. Sinskey, (Massachusetts Institute of Technology, Cambridge, Mass.) *US Patent 4,810,646*, **1989**.
[75] J. Bacon, V. Farmer, D. Jones, I. F. Taylor, *Biochem. J.* **1969**, *114*, 557.
[76] K. V. Clemons, M. E. Danielson, K. S. Michel, M. Liu, N. C. Ottoson, S. M. Leonardo, M. Martinez, V. Chen, M. A. Antonysamy, D. A. Stevens, *J. Med. Microbiol.* **2014**, *63*, 1750.
[77] L. Zhu, Z. Lei, X. Xia, Y. Zhang, Y. Chen, B. Wang, J. Li, G. Li, G. Yang, G. Cao, Z. Yin, *ACS Appl. Mater. Interfaces* **2021**, *13*, 40415.
[78] H. Huang, G. R. Ostroff, C. K. Lee, S. Agarwal, S. Ram, P. A. Rice, C. A. Specht, S. M. Levitz, *J. Immunol.* **2012**, *189*, 312.
[79] S. W. Howland, T. Tsuji, S. Gnjatic, G. Ritter, L. J. Old, K. D. Wittrup, *J. Immunother.* **2008**, *31*, 607.
[80] V. K. Berner, D. Redelman, K. W. Hunter, *Cell. Immunol.* **2015**, *298*, 104.
[81] a) K. Baert, B. G. De Geest, R. De Rycke, A. B. Da Fonseca Antunes, H. De Greve, E. Cox, *J. Control. Rel.* **2015**, *220*, 149; b) E. R. Soto, G. R. Ostroff, *Bioconjugate Chem.* **2008**, *19*, 840.
[82] M. Musick, X. Yu, *Immunol. Res.* **2023**, *71*, 197.
[83] X. Feng, Q. Xie, H. Xu, T. Zhang, X. Li, Y. Tian, H. Lan, L. Kong, Z. Zhang, *ACS Appl. Mater. Interfaces* **2022**, *14*, 31085.
[84] Y. Wu, C. Zhong, T. Du, J. Qiu, M. Xiong, Y. Hu, Y. Chen, Y. Li, B. Liu, Y. Liu, B. Zou, S. Jiang, M. Gou, *J. Drug Delivery Sci. Technol.* **2018**, *45*, 442.
[85] Y. Hou, L. Zhu, X. Ye, Q. Ke, Q. Zhang, X. Xie, J.-g. Piao, Y. Wei, *J. Nanobiotechnol.* **2024**, *22*, 305.
[86] a) B. Pulendran, P. S. Arunachalam, D. T. O'Hagan, *Nat. Rev. Drug Discovery* **2021**, *20*, 454; b) J. Aguilar, E. Rodriguez, *Vaccine* **2007**, *25*, 3752.
[87] H. Xu, R. F. Alzhrani, Z. N. Warnken, S. G. Thakkar, M. Zeng, H. D. Smyth, R. O. Williams III, Z. Cui, *Mol. Pharmaceutics* **2020**, *17*, 3259.
[88] J. A. M. Rodriguez, M. Bifano, E. Roca Goma, C. M. Plasencia, A. O. Torralba, M. S. Font, P. R. Millán, *Nutrients* **2021**, *13*, 4347.
[89] a) D. L. Williams, A. Mueller, W. Browder, *Clin. Immunother.* **1996**, *5*, 392; b) D. B. Zeković, S. Kwiatkowski, M. M. Vrvić, D. Jakovljević, C. A. Moran, *Crit. Rev. Biotechnol.* **2005**, *25*, 205.
[90] A. Albanese, W. C. Chan, *ACS Nano* **2011**, *5*, 5478.
[91] a) A. Rajabi, M. Nejati, M. Homayoonfal, A. Arj, Z. S. Razavi, A. Ostadian, B. Mohammadzadeh, M. Vosough, M. Karimi, N. Rahimian, *Int. J. Biol. Macromol.* **2024**, *260*, 128949; b) M. Lin, Y. Li, H. Long, Y. Lin, Z. Zhang, F. Zhan, M. Li, C. Wu, Z. Liu, *Int. J. Biol. Macromol.* **2023**, *225*, 873.
[92] a) C. Wu, B. Chu, L. Kuang, B. Meng, X. Wang, S. Tang, *Carbohydr. Polym.* **2013**, *98*, 807; b) J. Huang, C. Wu, S. Tang, P. Zhou, J. Deng, Z. Zhang, Y. Wang, Z. Wang, *Int. J. Nanomed.* **2020**, *15*, 5083.
[93] X. Zhang, Q. Hu, X. He, X. Cui, Z. Liang, L. Wang, X. Deng, Z. Zhang, W. Sheng, X. D. Han, *J. Nanobiotechnol.* **2023**, *21*, 159.
[94] Z. Zhang, M. Ge, D. Wu, W. Li, W. Chen, P. Liu, H. Zhang, Y. Yang, *Carbohydr. Polym.* **2024**, *332*, 121916.
[95] M. Sessevmez, G. Sinani, A. Okyar, H. O. Alpar, E. Cevher, *J. Drug Delivery Sci. Technol.* **2023**, 104704.

[96] R. Ravindran, K. Mitra, S. K. Arumugam, M. Doble, *Carbohydr. Polym.* **2021**, *258*, 117686.
[97] J.-K. Yan, Y.-Y. Wang, W.-Y. Qiu, J.-Y. Wu, *Carbohydr. Polym.* **2017**, *174*, 209.
[98] Y. Chen, Y. Wang, Z. Li, H. Jiang, W. Pan, M. Liu, W. Jiang, X. Zhang, F. Wang, *Int. J. Biol. Macromol.* **2024**, *276*, 133733.
[99] R. Liu, S. Fei, X. Zhang, Z. Hua, M. Tan, *Chem. Eng. J.* **2024**, *479*, 147590.
[100] J. W. Jin, S. Q. Tang, M. Z. Rong, M. Q. Zhang, *Acta Biomater.* **2018**, *78*, 211.
[101] J. W. Jin, M. Z. Rong, M. Q. Zhang, W. L. Wong, *J. Biomed. Mater. Res., Part A* **2021**, *109*, 2506.
[102] A. S. Cordeiro, Y. Farsakoglu, J. Crecente-Campo, M. de la Fuente, S. F. González, M. J. Alonso, *Drug Delivery Transl. Res.* **2021**, *11*, 1689.
[103] H. Zhang, K. Ma, H. Liu, S. Wang, Z. Wang, J. Zhang, J. Chen, *ACS Appl. Nano Mater.* **2023**, *6*, 22480.
[104] a) J. Han, J. Cai, W. Borjihan, T. Ganbold, T. M. Rana, H. Baigude, *Carbohydr. Polym.* **2015**, *117*, 324; b) J. Han, X. Wang, L. Liu, D. Li, S. Suyaola, T. Wang, H. Baigude, *Carbohydr. Polym.* **2017**, *163*, 191.
[105] V. K. Pawar, Y. Singh, K. Sharma, A. Shrivastav, A. Sharma, A. Singh, J. G. Meher, P. Singh, K. Raval, H. K. Bora, D. Datta, J. Lal, M. K. Chourasia, *Pharm. Res.* **2017**, *34*, 1857.
[106] B. Duan, S. Zou, Y. Sun, X. Xu, *Carbohydr. Polym.* **2021**, *254*, 117476.
[107] a) J. Minari, S. Mochizuki, T. Matsuzaki, Y. Adachi, N. Ohno, K. Sakurai, *Bioconjugate Chem.* **2011**, *22*,. b) S. Mochizuki, H. Morishita, K. Kobiyama, T. Aoshi, K. J. Ishii, K. Sakurai, *J. Control. Rel.* **2015**, *220*, 495.
[108] K. Lee, D. Min, Y. Choi, S. Yoon, J. Jang, J. Hwang, H. Jeon, Y. W. Cho, J. Choi, *Biomedicines* **2020**, *8*, 497.
[109] M. Ikeda, T. Hasegawa, M. Numata, K. Sugikawa, K. Sakurai, M. Fujiki, S. Shinkai, *J. Am. Chem. Soc.* **2007**, *129*, 3979.
[110] J. Hwang, K. Lee, A. A. Gilad, J. Choi, *Biotechnol. Bioprocess Eng.* **2018**, *23*, 144.
[111] a) Q. Liu, X. Xu, L. Zhang, J. Yu, *Eur. Polym. J.* **2012**, *48*, 1329; b) T. Anada, R. Karinaga, K. Koumoto, M. Mizu, T. Nagasaki, Y. Kato, K. Taira, S. Shinkai, K. Sakurai, *J. Control.Rel.* **2005**, *108*, 529; c) T. Anada, H. Matsunaga, R. Karinaga, K. Koumoto, M. Mizu, K. Nakano, S. Shinkai, K. Sakurai, *Bioorg. Med. Chem. Lett.* **2004**, *14*, 5655; d) S. Mochizuki, K. Sakurai, *J. Control. Rel.* **2011**, *151*, 155.
[112] D. Wu, L. Zhu, Y. Li, X. Zhang, S. Xu, G. Yang, T. Delair, *Carbohydr. Polym.* **2020**, *238*, 116126.
[113] a) R. Kaur, M. Sharma, D. Ji, M. Xu, D. Agyei, *Fibers* **2019**, *8*, 1; b) M. Wang, L. Zhang, R. Yang, C. Fei, X. Wang, K. Zhang, C. Wang, W. Zheng, F. Xue, *Int. J. Biol. Macromol.* **2016**, *93*, 203.
[114] a) T. Sasaki, N. Abiko, K. Nitta, N. Takasuka, Y. Sugino, *Eur. J. Cancer (1965-1981)* **1979**, *15*, 211; b) Z. Osawa, T. Morota, K. Hatanaka, T. Akaike, K. Matsuzaki, H. Nakashima, N. Yamamoto, E. Suzuki, H. Miyano, T. Mimura, *Carbohydr. Polym.* **1993**, *21*, 283; c) Y. Gao, A. Fukuda, K. Katsuraya, Y. Kaneko, T. Mimura, H. Nakashima, T. Uryu, *Macromolecules* **1997**, *30*, 3224; d) Q. Wang, S. Chen, L. Han, M. Lian, Z. Wen, T. Jiayinaguli, L. Liu, R. Sun, Y. Cao, *Int. J. Biol. Macromol.* **2014**, *69*, 229; e) Y. Adachi, N. Ohno, M. Ohsawa, S. Oikawa, T. Yadomae, *Chem. Pharm. Bull.* **1989**, *37*, 1838.
[115] a) V. Kafil, Y. Omidi, *BioImpacts: BI* **2011**, *1*, 23; b) S. Taranejoo, J. Liu, P. Verma, K. Hourigan, *J. Appl. Polym. Sci.* **2015**, 132.
[116] a) E. Boedtkjer, S. F. Pedersen, *Annu. Rev. Physiol.* **2020**, *82*, 103; b) L. Feng, Z. Dong, D. Tao, Y. Zhang, Z. Liu, *Natl. Sci. Rev.* **2018**, *5*, 269.
[117] a) V. S. Meka, M. K. Sing, M. R. Pichika, S. R. Nali, V. R. Kolapalli, P. Kesharwani, *Drug Discovery Today* **2017**, *22*, 1697; b) Y. Zhang, E. Yildirim, H. S. Antila, L. D. Valenzuela, M. Sammalkorpi, J. L. Lutkenhaus, *Soft Matter* **2015**, *11*, 7392.
[118] H. Vu-Quang, M. Muthiah, H. J. Lee, Y. K. Kim, J. H. Rhee, J. H. Lee, C. S. Cho, Y. J. Choi, Y. Y. Jeong, I. K. Park, *Carbohydr. Polym.* **2012**, *87*, 1159.
[119] a) N. T. Dung, T. D. Trong, N. T. Vu, N. T. Binh, T. T. L. Minh, L. Q. Luan, *Nanomaterials* **2021**, *11*, 2439; b) K. R. Trabbic, K. A. Kleski, J. J. Barchi Jr, *ACS Bio. Med. Chem. Au* **2021**, *1*, 31.
[120] A. Dube, J. L. Reynolds, W.-C. Law, C. C. Maponga, P. N. Prasad, G. D. Morse, *Nanomedicine: NBM* **2014**, *10*, 831.
[121] a) E. Soares, R. Cordeiro, H. Faneca, O. Borges, *Int. J. Biol. Macromol.* **2019**, *122*, 930; b) D. J. Cox, (Biothera, Inc.) *U.S. Patent US7981447B2*, **2011**.
[122] P. K. Singh, A. K. Srivastava, A. Dev, B. Kaundal, S. Roy Choudhury, S. Karmakar, *Carbohydr. Polym.* **2018**, *180*, 365.
[123] W. Guo, X. Zhang, L. Wan, Z. Wang, M. Han, Z. Yan, J. Li, R. Deng, S. Li, Y. Mao, *J. Pharm. Anal.* **2024**, 100953,.
[124] M. Tukulula, R. Hayeshi, P. Fonteh, D. Meyer, A. Ndamase, M. T. Madziva, V. Khumalo, P. Lubuschagne, B. Naicker, H. Swai, *Pharm. Res.* **2015**, *32*, 3119.
[125] a) C. Fei, L. Liu, H. Qi, Y. Peng, J. Han, C. Wang, X. Li, *ACS Appl. Mater. Interfaces* **2024**, *16*, 5536,. b) Y. Pan, Y. Qi, C. Fei, Z. Feng, Y. Ma, C. Wang, J. Han, *Macromol. Rapid Commun.* **2024**, *45*, 2400240.
[126] T. Cheng, T. Yan, J. Wu, Q. Wang, H. Zhang, *Int. J. Biol. Macromol.* **2023**, *234*, 123432.
[127] a) T. Lima, S. B. Gunnarsson, E. Coelho, D. V. Evtuguin, A. Correia, M. A. Coimbra, T. Cedervall, M. Vilanova, *Nanomaterials* **2022**, *12*, 2475; b) N. Bose, L. R. Wurst, A. S. Chan, C. M. Dudney, M. L. LeRoux, M. E. Danielson, P. M. Will, S. E. Nodland, M. L. Patchen, J. J. Dalle Lucca, *Glycobiology* **2014**, *24*, 379.
[128] Y.-B. Miao, H.-X. Ren, G. Zhang, F.-X. Song, W. Liu, Y. Shi, *Chem. Eng. J.* **2024**, *481*, 148520.
[129] Y. Wang, W. Song, S. Xue, Y. Sheng, B. Gao, Y. Dang, Y. Zhang, G. Zhang, *Int. J. Biol. Macromol.* **2024**, *276*, 133805.
[130] B. Fu, J. Hu, A. Yu, Y. Wang, *Adv. Funct. Mater.* **2024**, *34*, 2307823.
[131] K. H. Chen, N. Nguyen, T. Y. Huang, Y. J. Lin, Y. T. Yu, H. L. Song, J. T. Wang, V. K. Nguyen, H. L. Chen, L. A. Chu, *Adv. Mater.* **2023**, *35*, 2304735.
[132] R. Y. Basha, G. Venkatachalam, T. S. Kumar, M. Doble, *Mater. Sci. Eng. C* **2020**, *108*, 110379.
[133] E. Pandi, B. F. Proskhan, S. Kunjiappan, K. Sundar, V. Balakrishnan, *J. Polym. Environ.* **2024**, *32*, 3071.
[134] H. Chen, Y. Sun, X. Xu, Q. Ye, *Carbohydr. Polym.* **2022**, *284*, 119183.
[135] Y. Su, F. Yang, L. Chen, P. C. Cheung, *J. Agric. Food Chem.* **2022**, *70*, 7110.
[136] X. Ling, Z. Tian, D. Chen, Y. Zhang, Z. Dong, D. He, J. Li, Z. He, J. Li, F. Chen, *J. Control. Rel.* **2025**, *378*, 559.
[137] B. W. Ebeed, I. A. Abdelmawgood, M. A. Kotb, N. A. Mahana, A. S. Mohamed, M. A. Ramadan, A. M. Badr, M. Nasr, O. M. Qurani, R. M. Hamdy, *Apoptosis* **2024**, *30*, 35.
[138] R. Y. Basha, S. K. TS, M. Doble, *Carbohydr. Polym.* **2019**, *218*, 53.
[139] J. Heo, T. A. Sobiech, H. L. Kutscher, L. Chaves, D. K. Sukumaran, S. Karki, A. Dube, P. N. Prasad, J. L. Reynolds, *Macromol. Biosci.* **2021**, *21*, 2000358.
[140] a) M. Colaç, A. P. Marques, S. Jesus, A. Duarte, O. Borges, *Chem. Res. Toxicol.* **2020**, *33*, 915; b) T. Roquito, M. Colaço, J. P. Costa, O. Borges, *Colloids Surf., B* **2025**, *245*, 114326.
[141] A. C. Wauters, J. F. Scheerstra, M. M. van Leent, A. J. Teunissen, B. Priem, T. J. Beldman, N. Rother, R. Duivenvoorden, G. Prévot, J. Munitz, *Nat. Nanotechnol.* **2024**, *19*, 1735.
[142] F. Yang, Y. Su, C. Yan, T. Chen, P. C. K. Cheung, *J. Nanobiotechnol.* **2024**, *22*, 166.
[143] Y. B. Miao, K. H. Chen, C. T. Chen, F. L. Mi, Y. J. Lin, Y. Chang, C. S. Chiang, J. T. Wang, K. J. Lin, H. W. Sung, *Adv. Mater.* **2021**, *33*, 2100701.

[144] V. K. Nguyen, N. Nguyen, Z. C. Li, C. M. Cheng, J. T. Wang, Y. W. Chiang, H. L. Song, S. K. Lo, C. H. Mac, Y. Chang, *Adv. Funct. Mater.* **2024**, *34*, 2401570.
[145] P. K. Luo, H. M. Ho, M. C. Chiang, L. A. Chu, Y. H. Chuang, P. C. Lyu, I. C. Hu, W. A. Chang, S. Y. Peng, J. Jayakumar, *Adv. Mater.* **2024**, *36*, 2404830.
[146] H. Kim, S. Lee, C. S. Ki, *Carbohydr. Polym.* **2021**, *252*, 117132.
[147] a) T. R. Hoare, D. S. Kohane, *Polymer* **2008**, *49*, 1993; b) M. A. Campea, M. J. Majcher, A. Lofts, T. Hoare, *Adv. Funct. Mater.* **2021**, *31*, 2102355.
[148] N. Miyamoto, S. Mochizuki, S. Fujii, K. Yoshida, K. Sakurai, *Bioconjugate Chem.* **2017**, *28*, 565.
[149] Z. Nasrollahi, S. R. Mohammadi, E. Mollarazi, M. H. Yadegari, Z. M. Hassan, F. Talaei, R. Dinarvand, H. Akbari, F. Atyabi, *J. Control. Rel.* **2015**, *202*, 49.
[150] N. Nguyen, T.-M. Hoang, T.-Y. Huang, H.-H. Chang, Y. Chang, M. T. T. Nguyen, K.-J. Lin, C.-C. Chen, H.-W. Sung, *Biomaterials* **2025**, *316*, 123019.
[151] A. Song, Y. Wang, J. Xu, X. Wang, Y. Wu, H. Wang, C. Yao, H. Dai, Y. Zhang, Q. Wang, *Nano Today* **2024**, *54*, 102109.
[152] R. Zhang, X. Qin, J. Lu, H. Xu, S. Zhao, X. Li, C. Yang, L. Kong, Y. Guo, Z. Zhang, *ACS Appl. Mater. Interfaces* **2023**.
[153] a) P. Kankkunen, L. Teirilä, J. Rintahaka, H. Alenius, H. Wolff, S. Matikainen, *J. Immunol.* **2010**, *184*, 6335; b) S. V. Tsoni, G. Brown, *Ann. N. Y. Acad. Sci.* **2008**, *1143*, 45; c) S. Walachowski, G. Tabouret, G. Foucras, *PLoS One* **2016**, 0148464.
[154] H. Yue, G. Ma, *Vaccine* **2015**, *33*, 5927.
[155] D. Wibowo, S. H. Jorritsma, Z. J. Gonzaga, B. Evert, S. Chen, B. H. Rehm, *Biomaterials* **2021**, *268*, 120597.
[156] H. Liang, X. Xiao, X. Zhang, Q. Hu, Y. Yang, S. Cen, X. Deng, W. Sheng, *Biochem. Biophys. Res. Commun.* **2019**, *511*, 253.
[157] S. Zhang, H. Jiang, S. Huang, P. Li, F. Wang, *Carbohydr. Polym.* **2019**, *213*, 100.
[158] S. D'Souza, S. Du Plessis, S. Egieyeh, R. Bekale, R. Maphasa, A. Irabin, S. Sampson, A. Dube, *J. Pharm. Sci.* **2022**, *111*, 469.
[159] H. Chen, N. Liu, S. Hu, X. Li, F. He, L. Chen, X. Xu, *Carbohydr. Polym.* **2024**, *342*, 122401.
[160] A. Donadei, S. Gallorini, F. Berti, D. T. O'Hagan, R. Adamo, B. C. Baudner, *Mol. Pharmaceutics* **2015**, *12*, 1662.
[161] J. Ajit, B. Cassaidy, S. Tang, A. Solanki, Q. Chen, J. Shen, A. P. Esser Kahn, *Adv. Healthcare Mater.* **2022**, *11*, 2200819.
[162] a) A. Mueller, J. Raptis, P. J. Rice, J. H. Kalbfleisch, R. D. Stout, H. E. Ensley, W. Browder, D. L. Williams, *Glycobiology* **2000**, *10*, 339; b) J. Wang, L. Zhang, Y. Yu, P. C. Cheung, *J. Agric. Food Chem.* **2009**, *57*, 10565.
[163] a) Y. Tanaka, M. Nishikawa, Y. Mizukami, K. Kusamori, Y. Ogino, S. Nishimura, K. Shimizu, S. Konishi, Y. Takahashi, Y. Takakura, *J. Control. Rel.* **2018**, *270*, 177; b) N. Bidan, G. Dunsmore, M. Ugrinic, M. Bied, M. Moreira, C. Deloménie, F. Ginhoux, C. Blériot, M. de la Fuente, S. Mura, *Drug Delivery Transl. Res.* **2024**, *14*, 2085.

Nate Dowdall is currently pursuing a PhD in Chemical Engineering at McMaster University under the supervision of Dr. Todd Hoare after completing his B.A.Sc. at Queen's University in 2019. His current research focuses on the design of immunomodulatory yeast beta-glucan micro/nanoparticles for the treatment of cancer and fibrotic diseases.

Todd Hoare is a Professor and the Canada Research Chair in Engineered Smart Materials in the Department of Chemical Engineering at McMaster University. He completed his B.A.Sc. at Queen's University in 2001, his Ph.D. at McMaster University in 2006, and a postdoctoral fellowship in Robert Langer's lab at the Massachusetts Institute of Technology in 2008. His lab develops hydrogels on multiple length scales for applications in medicine, agriculture, and personal care products.